Calibration of Scanning Lidar Molas 3D units #27 and #28

Mathieu Pellé (Measurement Engineer)
Elliot Simon (Measurement Engineer and Review)

Abstract

This report presents the result of the line-of-sight calibration performed for two Movelaser Molas3D scanning lidars (units 27 and 28), at DTU Risø Campus, Denmark. Calibration is here understood as the establishment of a relation between the reference wind speed measurements, provided by measurement standards, and the corresponding lidar line-of-sight (LOS) wind speed indications. The lidar calibration concerns the 10-minute mean LOS wind speed measurements.

The evaluated data cover the measurement period from 03-Nov-2023 11:00 to 27-Nov-2023 03:10.

Total number of pages: 40

Revision history:

Revision No.	Date	Reason for Issue
R0	06/02/2024	First version

Name and address of client:

Nanjing Movelaser Co., Ltd
Building D4
Hongfeng Science Park, Qixia District
21000, Nanjing City
Jiangsu Province, China

Name and address of measurement laboratory:

DTU Wind Energy
Building 118
P.O. Box 49
Risø Campus
Frederiksborgvej 399
DK-4000 Roskilde
Denmark

Internal Review	Measurement Engineer

Contents

1. Introduction

This report documents the calibration of Molas 3D units 27 and 28. The calibration was carried out at DTU Risø Campus, in Denmark. The details of the tested lidar models are given below:

Lidar type	Pulsed Scanning Doppler wind lidar
Model number	Molas3D-O
Serial number (unit 27)	DO2023090027
Serial number (unit 28)	DO2023090028
Year of make	2023
Software version	Molas3D Service 2.3.9.0 and Molas3D 2.2.12.4

2. Timeline of events

This is a list of the most significant events during the testing and reporting.

- Lidars arrived at Risø on 03-Oct-2023
- Installation of lidars at test pads on 16-Oct-2023
- Hard target mapping on 27-Oct-2023
- LOS calibration:
    - Start of calibration: 03-Nov-2023 11:00
    - End of calibration: 27-Nov-2023 03:10

3. Test site and instrumentation

3.1 Location

The calibration took place at DTU Risø Campus, Roskilde, Denmark. As seen from Figure 3.1.1, the test site is situated within Zealand, on the south-east end of the Roskilde fjord. The test site comprises of a meteorological mast on the west side of the site, and a wind turbine test row on the south edge of the site (see Figure 3.1.2 and Figure 3.1.1). An aerial view of the area can be seen on Figure 3.1.3.

The reference instrumentation used for this calibration is the Risø mast. The two scanning lidars were installed close to test pad S1, approximately 1060m to the South-East of the met mast. The coordinates are summarised in Table 3.1.

Figure 3.1.1 Location of Risø test site (source: Google Earth).

Figure 3.1.2 Details of test site locations. (source: Google Earth)

Figure 3.1.3 Aerial view of DTU Risø Campus (source: DTU)

Table 3.1 Coordinates of relevant Risø test pads and Risø mast obtained from GPS measurements made with a laser theodolite.

	Coordinates (UTM 33 EUREF89)		Height above sea level	Distance to mast	Direction to mast
	E [m]	N [m]	[m]	[m]	[°]
Risø mast base	317000	6175890	7.1	-	-
S1	317548	6174985	10.9	1062	329

3.2 Reference instruments

The lidar measurements are compared with reference wind speed measurements from the met mast. The reference instrument is the 118m cup anemometer. Note that that all instrument heights are provided with respect to ground level.

The met mast is equipped with several other instruments which are used for control and filtering of the data. The cup anemometer at 44.1m is used together with the reference cup to estimate shear. The top wind vane, at 122.5m, is used as the main wind direction measurement and for the shear estimate with the wind vane at 76.5m. Turbulence intensity (TI) is computed using the standard deviation and average signal of the reference cup. A 3-D ultrasonic anemometer at 118m provides measurements of temperature as well as the three-components of the wind speed vector which are then used to calculate the inflow angle, the horizontal wind speed and the wind direction measurements. Environmental parameters such as temperature, pressure and relative humidity are also measured close to the reference cup height. The instruments used for nacelle lidar calibration are described in Table 3.2. A drawing of the met-mast setup is shown in Figure 3.2.1 and includes other instruments that were not used in this test. Figure 3.2.2 and Figure 3.2.3 show pictures of the met mast.

Table 3.2 Instrumentation of Risø mast used in this test.

Parameters	Sensor	Height from mast base
Horizontal wind speed	WindSensor Cup anemometer Type: P2546D-OPR Sn: 67079, PFV 1103-4667	118m
Horizontal wind speed	WindSensor Cup anemometer Type: P2546D-OPR Sn: 67075, PFV 1103-4663	44.1m
Wind direction	Vector W200P Wind vane	122.5m
Wind direction	Vector W200P Wind vane	76.5m
3 component wind speed, temperature	METEK USA-1 4 Basic Ultrasonic anemometer	118m
Relative humidity	Vaisala, HMP 155	117m
Atmospheric pressure	Vaisala, PTB110	117m
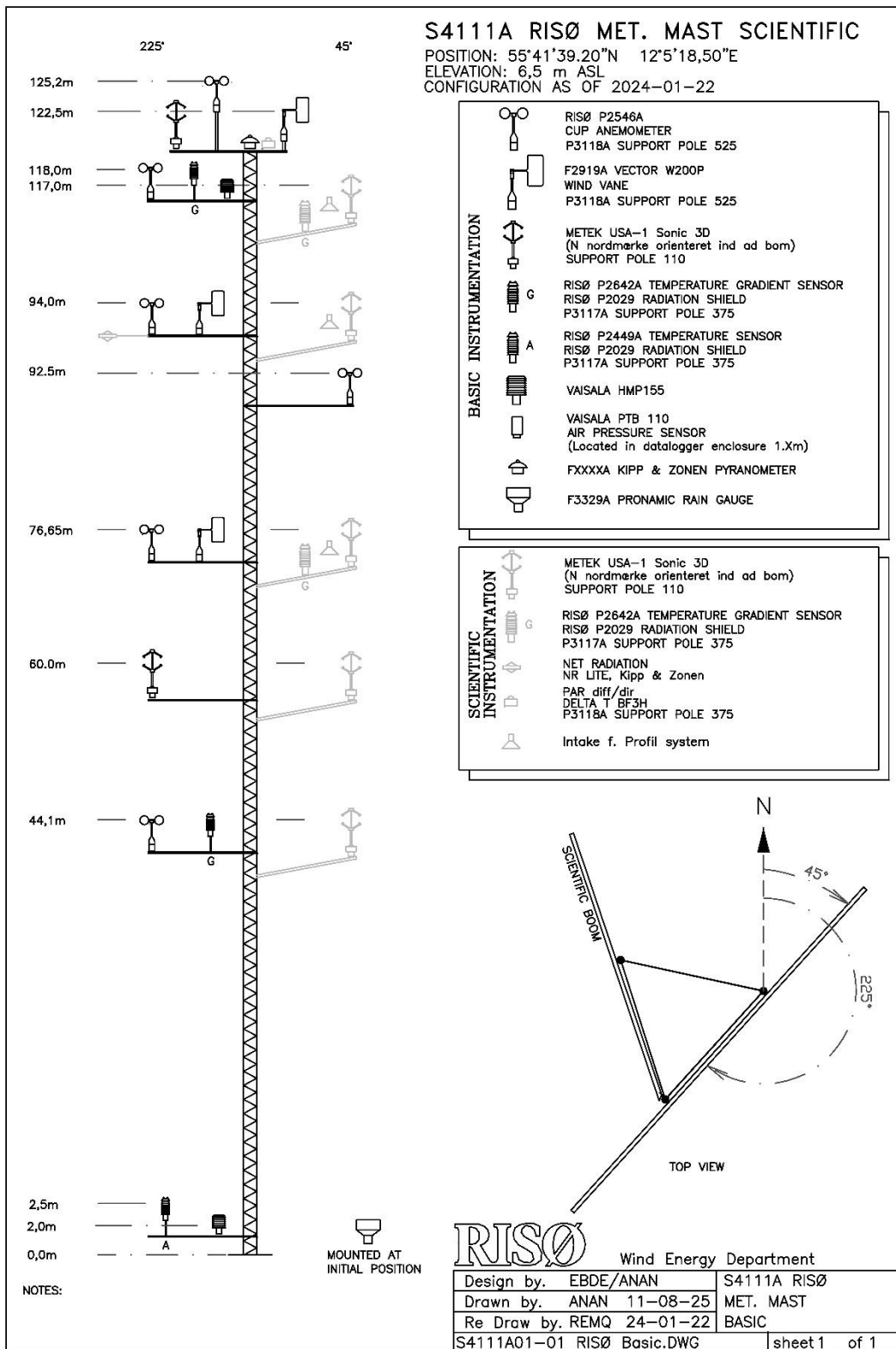
Figure 3.2.1 Drawing of Risø mast instrumentation.
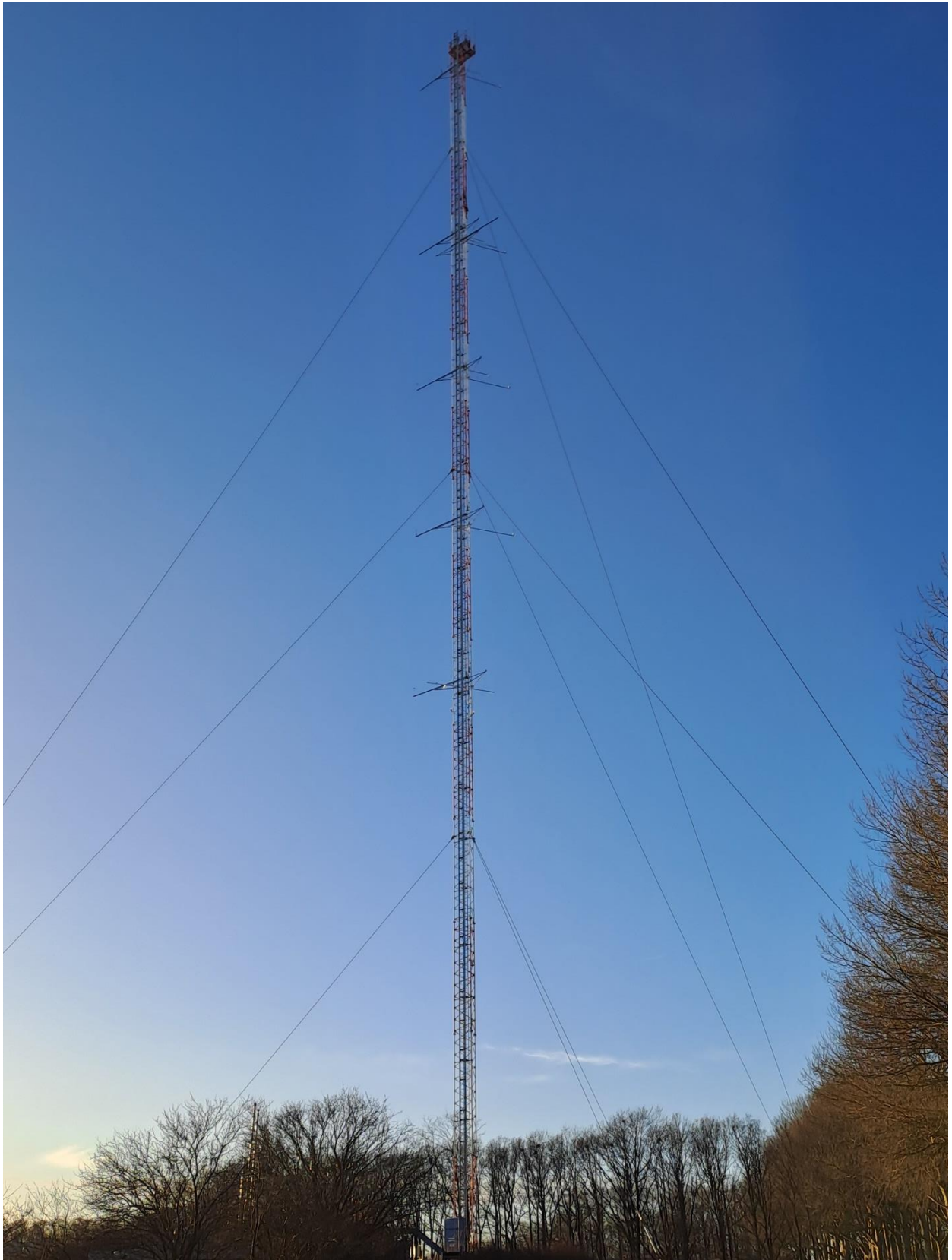
Figure 3.2.2 Risø mast (picture taken towards the fjord).

Figure 3.2.3 Met-mast top.

4. Measurement setup

4.1 Lidar positioning

The lidars were installed side by side on a platform near S1 (see Figure 4.1.1). As the lidars do not include an internal inclinometer, the levelling of the lidars was done by adjusting the feet of the lidar and checking the lidar's bubble level. The GPS positions were taken at the scan head's centre of rotation using a Leica Geosystems GS16 GNSS-RTK and CS20 Field Controller with a 3D position quality of 3 cm or better. The position measurements can be found in Table 4.1. The GPS position of the reference cup at 118m was also taken. The cup is approximately 1066m distance from the lidars along the beam path, at an azimuth angle of 329°.

The lidars were not physically aligned with true north when installed. A correction offset to the azimuth angle was therefore computed from the hard target mapping and applied in the lidar settings. This is explained in the following section.

Table 4.1 Coordinates of reference instrument and lidars.

	Coordinates (UTM 33 EUREF89)		Height above sea level	Distance to cup	Direction to cup	Elevation to cup
	E [m]	N [m]	[m]	[m]	[°]	[°]
118m Cup	316997.3	6175885.8	124.7	-	-	-
Molas 3D unit 27	317541.5	6174975.0	10.90	1066.5	329.19	6.12
Molas 3D unit 28	317539.3	6174974.5	10.88	1066.4	329.26	6.13

Figure 4.1.1 Lidar installation pad with view towards reference mast. Unit 27 is installed on the right and unit 28 on the left.

4.2 Hard target mapping

The hard target mapping is used to control the positioning (azimuth and elevation/pitch) of the lidar scanning head. Note that elevation angle is the term used in this report, but it is equivalent to the pitch input used in the lidar software. The lidar is programmed to perform PPI (Plan Position Indicator) scans at varying elevation angles whilst aiming at a hard target. The CNR signal is then used to visualize the hard target as a function of azimuth and elevation angles. The GPS positions found in Table 4.1 are then used to estimate the lidar's azimuth and elevation offsets.

The hard target used here is the top of Risø mast. With the help of Movelaser, PPI scans were programmed with the settings shown in Table 4.2. Note that the azimuth angle range is defined relative to the North mark of the lidar, comparing the mapping result to the GPS measurements will provide the lidar's azimuth offset to true North.

Table 4.2 Hard target mapping scan parameters.

Parameter	Value
Azimuth angle range [°]	[170, 173.5]
Azimuth angle step [°]	~0.02
Elevation angle range [°]	[3.5, 7.5]
Azimuth angle step [°]	~0.02
Range gates	Every 4m from 40m to 1232m

The lidar software does not include an integrated CNR mapper tool, so CNR contours were created by postprocessing the data from the PPI scans. Figure 4.2.1 shows the Figure 4.2.2 contours for lidar units 27 and 28 respectively. The position of the 118m cup was estimated from these contours and compared to the measured GPS positions. Table 4.3 summarises the results of the mapping. The azimuth angle from lidar to cup is given both in the lidar reference and in the compass reference, the difference being the installation offset. The elevation angle offset is obtained with the difference between the scanning

head elevation found from the mapping and the elevation angle found from the GPS measurements (Table 4.1).
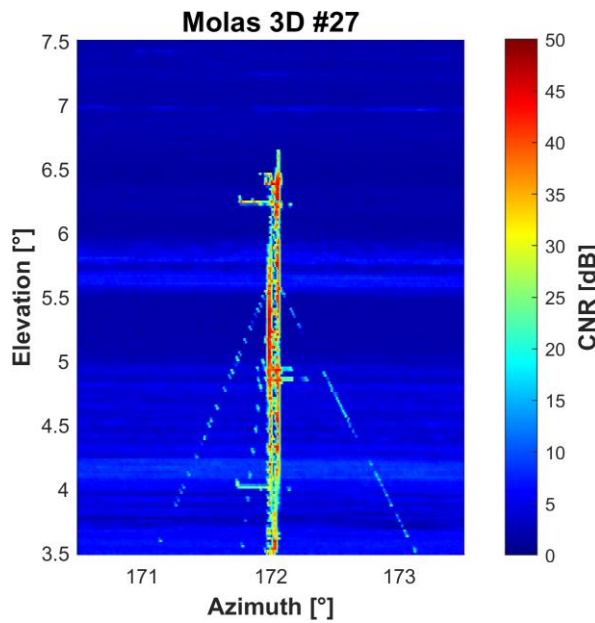
Figure 4.2.1 CNR contour from hard target mapping with Molas3D unit 27.
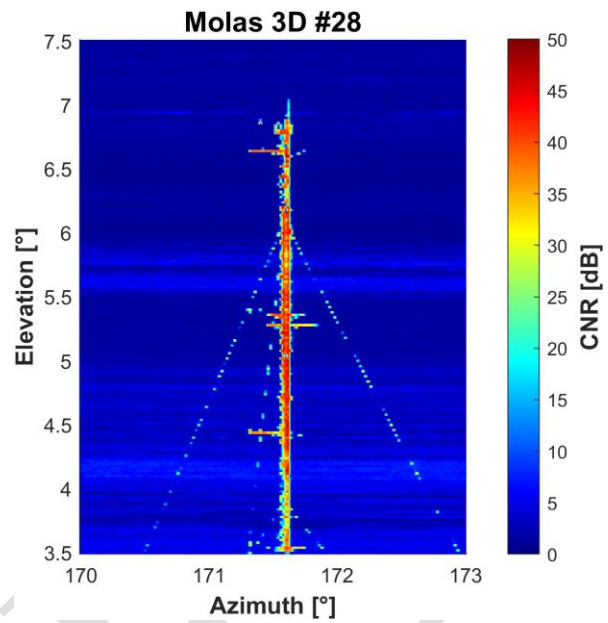
Figure 4.2.2 CNR contour from hard target mapping with Molas3D unit 28.

Table 4.3 Results of hard target mapping analysis.

Parameter	Molas 3D #27	Molas 3D #28
Installation offset to true North [°]	157.2	157.7
Cup azimuth angle [°] (relative to lidar orientation)	171.8	171.0
Cup azimuth angle [°] (relative to true North)	328.95	329.0
Cup elevation angle [°]	6.3	6.7
Elevation offset [°]	0.2	0.6
Range offset [m]	14	14

The range offset reported in Table 4.3 was estimated from the maximum CNR signal received from each range gate. Figure 4.2.3 and Figure 4.2.4 show the CNR against range for the azimuth and elevation angles at which the 118m cup was found from the CNR contours. For both lidars, the maximum CNR was found for the 1080m range gate. Compared to the expected 1066m range from the GPS measurements, this may indicate a range offset between 10m to 18m.
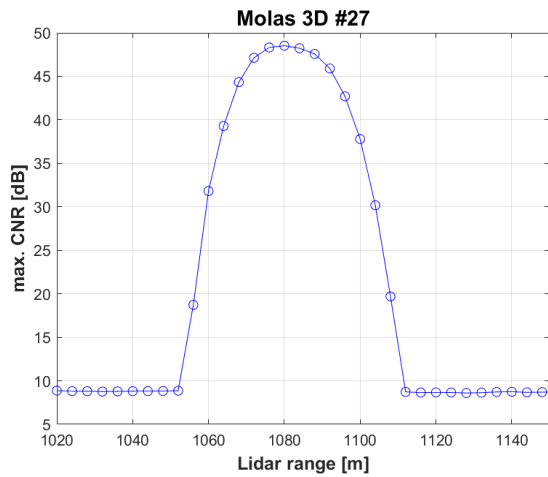
Figure 4.2.3 Maximum CNR against range during mapping of Molas3D unit 27.
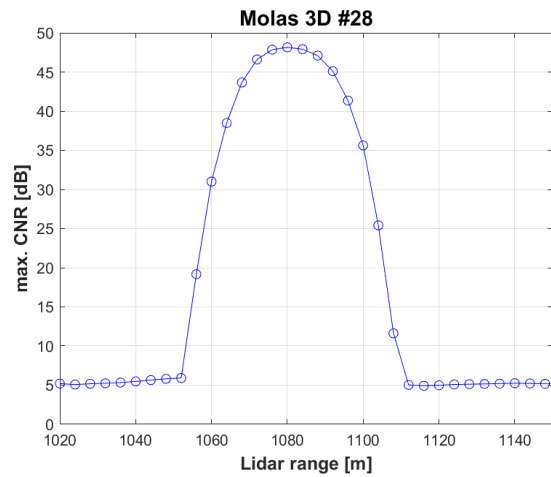
Figure 4.2.4 Maximum CNR against range during mapping of Molas3D unit 28.

4.3 Time synchronization

The lidars and reference instrument's data acquisition are synchronized to the same time NTP server. DTU's measurement system time is in UTC+1 and daylight savings time is never applied. The lidar PC was set to the same time zone and no time offset correction was therefore applied.

4.4 Lidar configuration

The LOS calibration is performed with the lidars in staring mode, at a fixed azimuth and elevation, pointing close to the reference cup. Molas 3D unit 27 was set up to measure slightly above the cup whilst Molas 3D unit 28 was set to measure at the same height but to the left of the cup. This was done to have both lidar beams parallel to one another and allow easier comparison of the performance of both lidars.

Table 4.4 Lidar settings for line-of-sight calibration.

Parameter	Molas 3D #27	Molas 3D #28
Azimuth angle [°]	328.95	328.95
Elevation angle [°]	6.35	6.75
Accumulation time [s]	1	
Pulse length [ns]	200	
Range gates	Every 5m from 150m to 1555m Every 100m from 1600m to 2000m Every 500m from 2000m to 8000m	

4.5 Data processing

The lidar data is read from time series ('RealTime') csv files produced by the Molas 3D lidar every day. Files are copied via remote access to the lidar's computer and data is uploaded to DTU's MySQL database for storage. 10-minute statistics of the data are calculated by DTU.

5. Procedure

In order to compare the line-of-sight speed measured by the lidar to the reference cup, a projection of the cup wind speed along the LOS direction must be performed. The first parts of this section will outline how this can be done. The final part of this section presents the various filtering criteria used in the data analysis.

5.1 Determining the line-of-sight direction

Although the line-of-sight direction is given geometrically by the positions of the mast and the lidar (assuming a perfect alignment), one can also determine this direction from the data. Figure 5.1.1 shows a plot of the 10-minute lidar LOS wind speeds normalized by the mean speed of the cup anemometer across the wind direction range. This is only shown here for lidar unit 28, but the identical process is applied to both lidars. The data is filtered for this analysis to ensure good data quality and a reliable LOS direction estimate. The filters applied are detailed in section 5.4. All but the wind direction filter have been applied here.
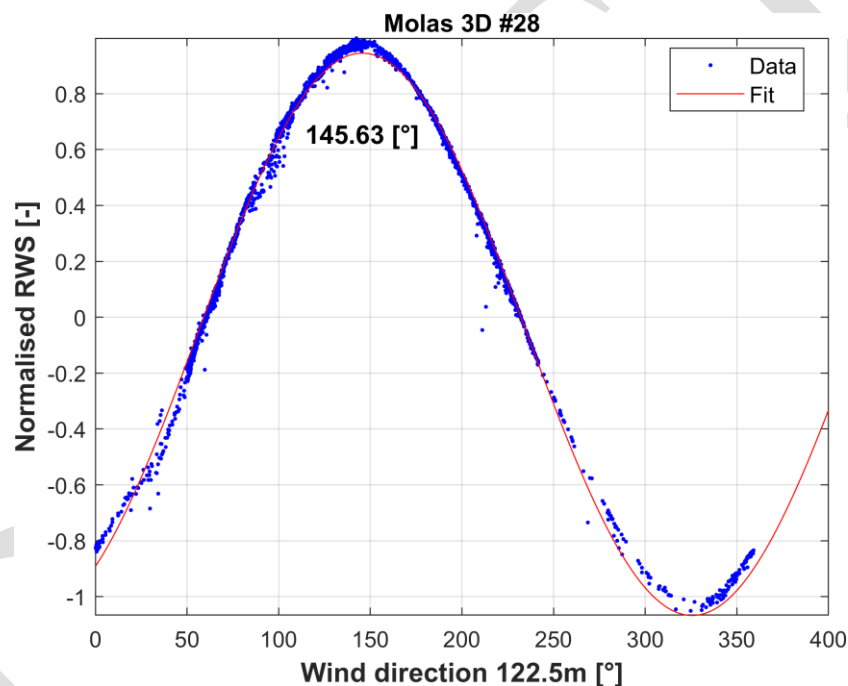
Figure 5.1.1 Normalised LOS speed plotted as a function of wind direction, used to estimate the LOS direction.

A maximum normalized radial wind speed occurs around 149.69° where the wind direction coincides with the lidar's line-of-sight. This value is used as a first estimate for the line-of-sight direction. A refined LOS direction estimate can be made by restricting the wind direction range to focus on the peak area. For this restricted dataset, a linear regression between the lidar's LOS wind speed and the projected cup wind speed is performed for several line-of-sight directions close to the first estimated value. For each regression (representing one specific line of sight direction), the sum of squares of the residuals is computed. The line-of-sight direction closest to the true value is assumed to have the lowest error due to misalignment and therefore the lowest residual. Figure 5.1.2 shows the result of this process for unit 27 and Figure 5.1.3 shows this for unit 28. One can see a smooth function closely approximating a parabola, from which the line-of sight (LOS) direction can be estimated. This is found as 145.99° for unit 27 and 145.44° for unit 28.
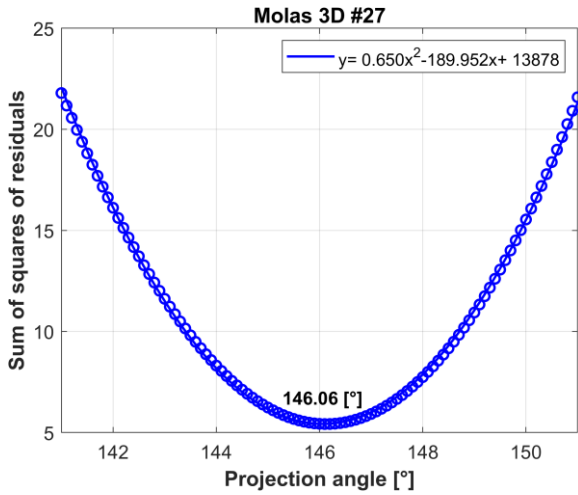
Figure 5.1.2 Refined LOS direction for Molas 3D unit 27
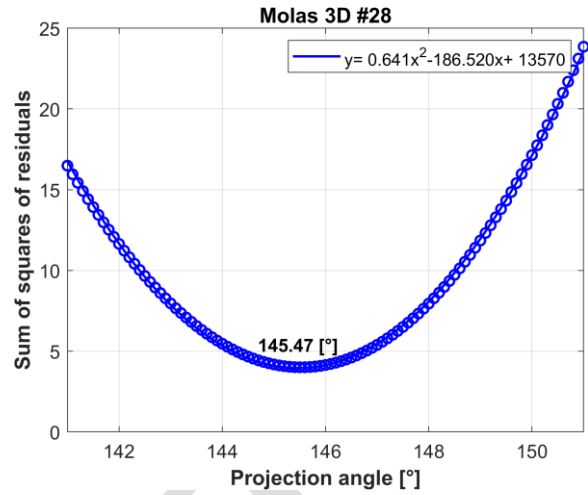
Figure 5.1.3 Refined LOS direction for Molas 3D unit 28

5.2 Beam elevation angle

The physical elevation of the lidar beam is also required to project the cup wind speed. The elevation angle (φ) was calculated from the GPS measurements taken at the location of the lidar and at the reference cup anemometer. This was estimated in Table 4.1 as 6.12° for unit 27 and 6.13° for unit 28.

5.3 Calibrating the LOS wind speed

The cup wind speed V_{hor} is projected along the line-of-sight direction (θ_{los}) using the 10-minute mean wind direction (θ) and the beam elevation angle (φ) as follows:

$$V_{ref} = V_{hor} * \cos(\theta - \theta_{los}) * \cos(\varphi)$$

This gives us V_{ref}, the cup wind speed projected onto the line-of-sight direction, which is then used as the reference wind speed for comparison to the lidar line-of-sight wind speed.

5.4 Data filtering

The following filters were applied on the time series dataset:

- CNR between 0.49dB and 15dB.
- Lidar error values (NaN) were excluded.

Data was then resampled to 10-minute statistics and the following filters were then applied:

- Wind direction at 122.5m height within -20° and 20° of LOS direction. Approximately [125°, 166°] and [305°, 346°] depending on the LOS direction obtained for each lidar.
- 118m cup anemometer wind speed between 4m/s and 16m/s, which is the wind speed calibration range of the cup anemometer.
- Lidar availability greater or equal to 400 samples per 10-minute.
- Temperature at 118m greater than 2°C to remove the possibility of icing on the cup anemometer.

The effect of these filters on the data will be shown for each lidar in sections 6.1.1 and 6.2.1.

6. Results

This section presents the results of the calibration for both lidar unit 27 and 28. For each lidar, the first section gives an overview of some of the conditions throughout the test and the effect of filtering on the dataset. The second section provides the linear regression against the reference instrument and the deviations against some of the measured environmental parameters. The third section shows results after the dataset has been binned into bins of 0.5m/s of the reference wind speed and provides the result of the uncertainty analysis. The procedure followed for the uncertainty analysis is provided in Appendix B.

6.1 Molas 3D Unit 27

6.1.1 Filtering effects

Figure 6.1.1 and Figure 6.1.2 show the effect of the CNR filter on the time series data of the Molas 3D unit 27. The blue points pass the filter, and the red ones are excluded by the filter.
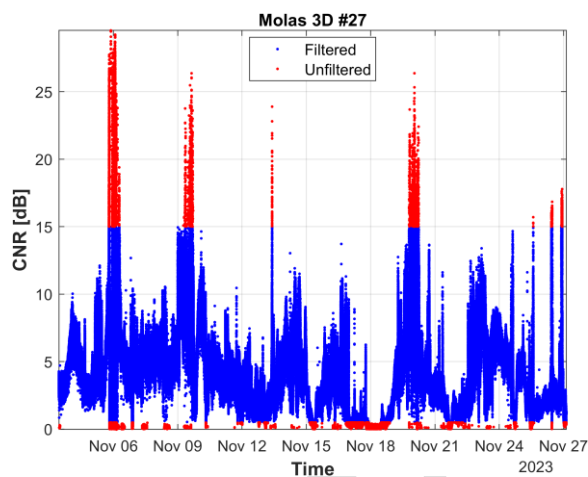
Figure 6.1.1 CNR filter.
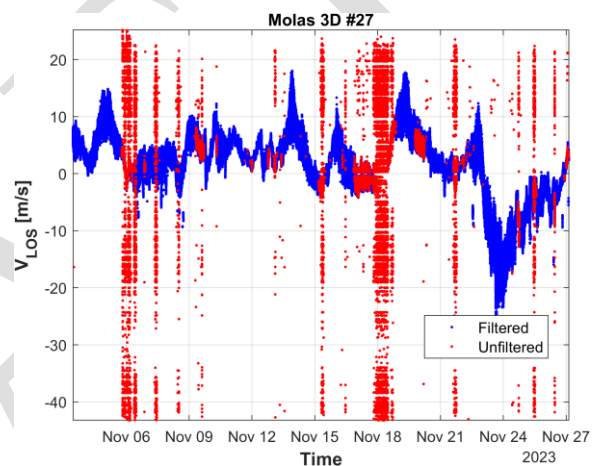
Figure 6.1.2 CNR filter effect on lidar LOS speed.

Figure 6.1.3 shows the independent effect of the wind speed filter on the data across the measurement period. The same is shown for temperature and wind direction in Figure 6.1.4 and Figure 6.1.5 respectively. Additionally, Figure 6.1.6 shows the lidar-cup deviation with varying wind direction to confirm the selected sector is valid.
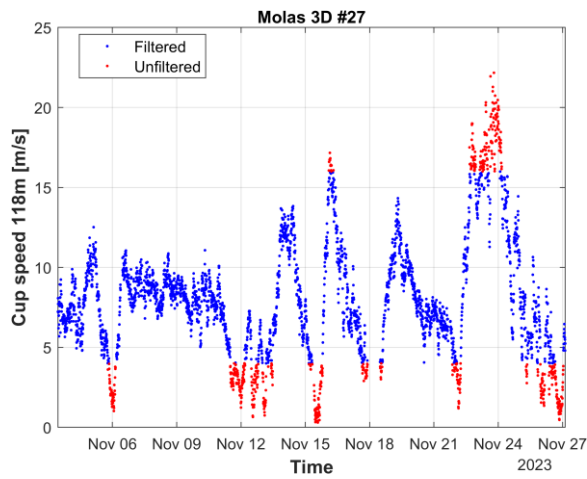
Figure 6.1.3 Cup wind speed filter.
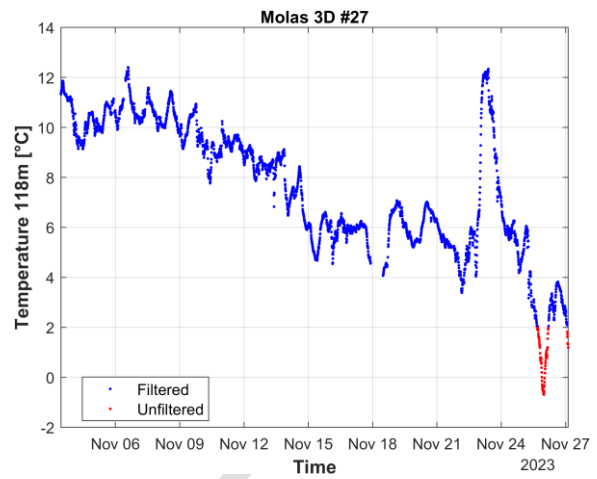
Figure 6.1.4 Temperature filter.
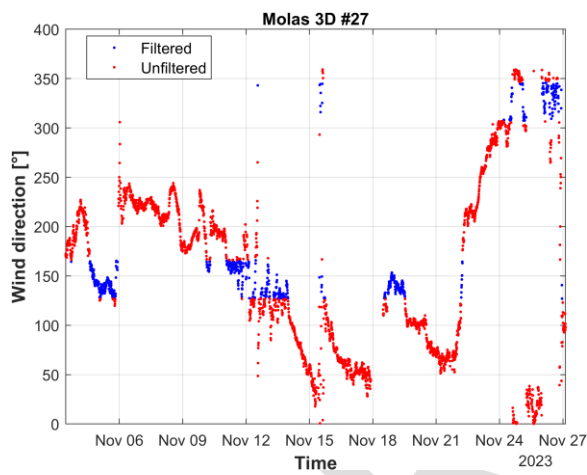
Figure 6.1.5 Wind direction filter.
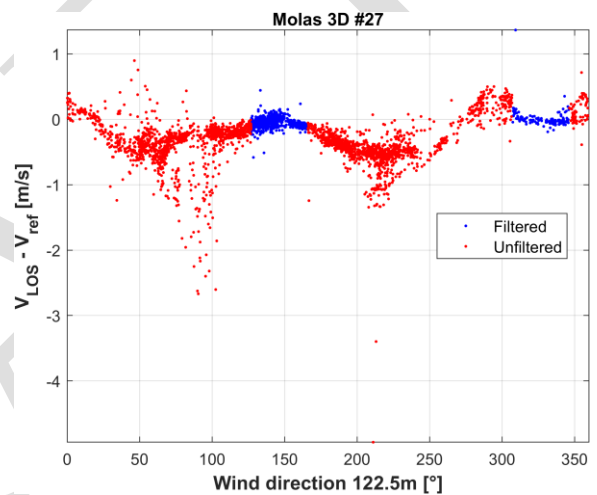
Figure 6.1.6 Wind direction filter and error.

Figure 6.1.7 shows the availability of the lidar over time. The filter was set to exclude 10-minute periods where less than 400 data samples were obtained by the lidar. Towards the end of the campaign, it was noticed that the sampling rate of lidar unit 27 decreased suddenly and did not return to its original level. This issue could not be solved during the measurement period and resulted in lower 10-minute data availability for the last 3 days of measurements.
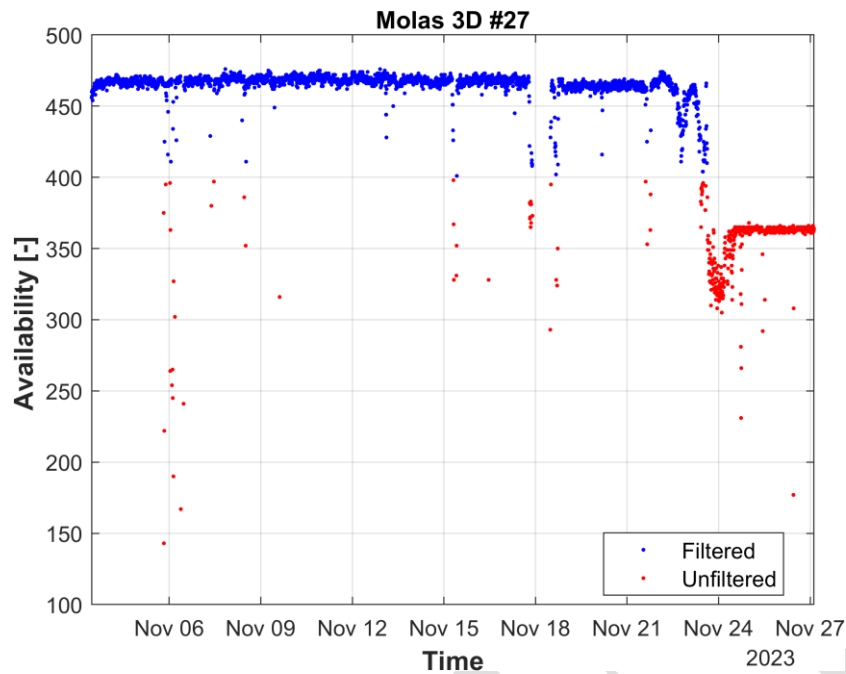
Figure 6.1.7 Lidar availability filter.

6.1.2 10-minute average dataset

Figure 6.1.8 shows the linear regression obtained between the lidar line-of-sight wind speed and the reference wind speed. The linear fit with and without forced y-intercept are also displayed, together with their respective coefficient of determination. Figure 6.1.9 to Figure 6.1.18 show how the deviation (lidar-cup) evolves with various measured parameters.
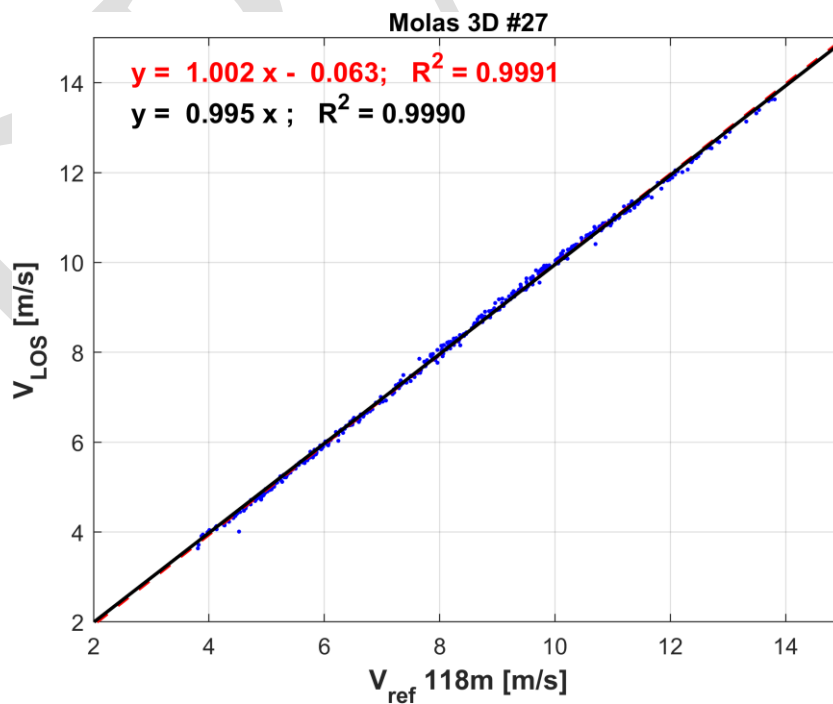
Figure 6.1.8 Linear regression of 10min. averages.
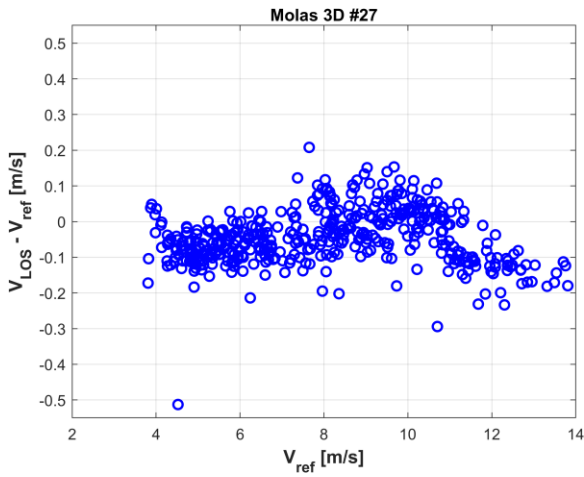
Figure 6.1.9 Deviations against reference wind speed.
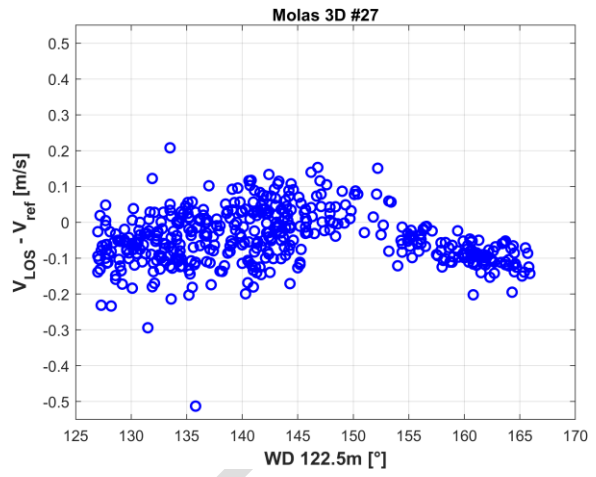
Figure 6.1.10 Deviations against wind direction.
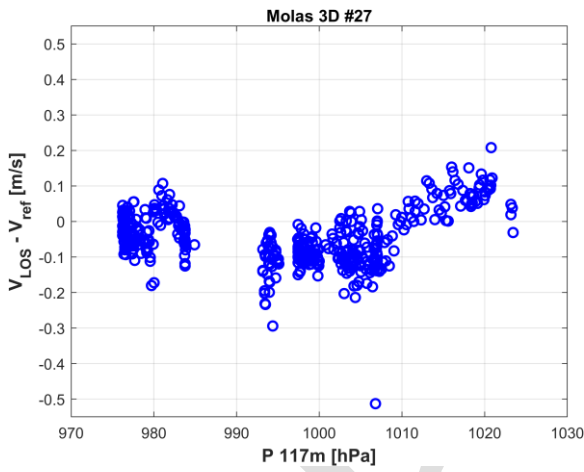
Figure 6.1.11 Deviations against air pressure.
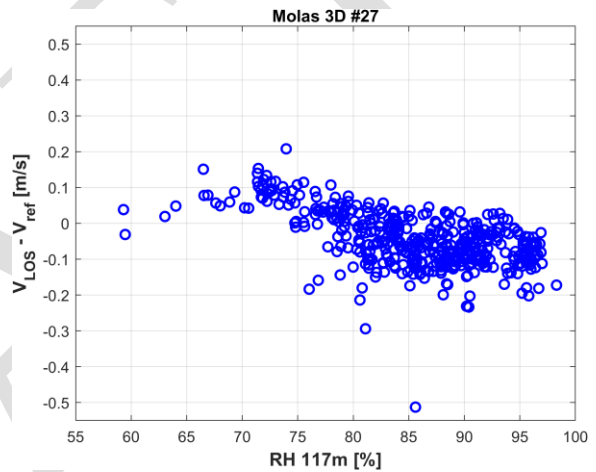
Figure 6.1.12 Deviations against relative humidity.
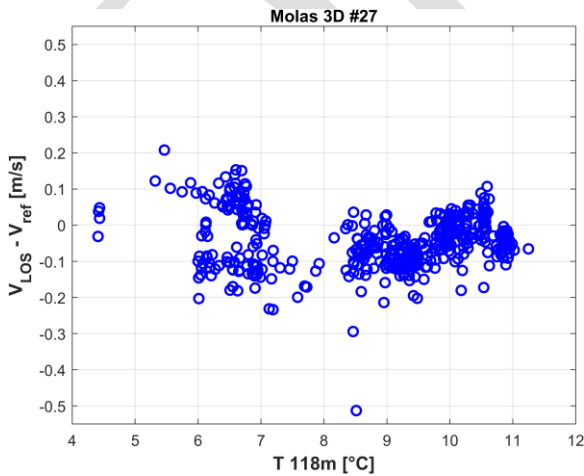
Figure 6.1.13 Deviations against temperature.
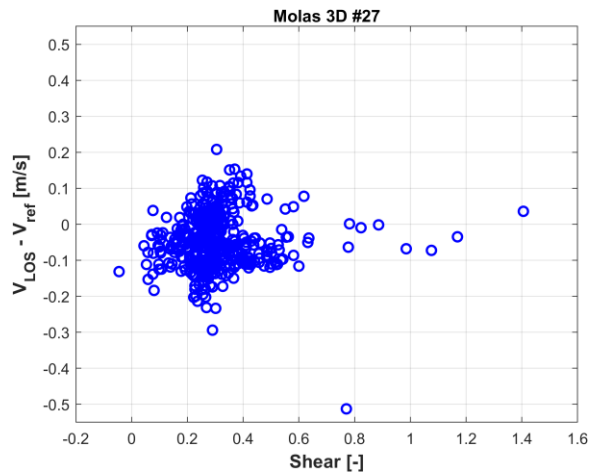
Figure 6.1.14 Deviations against shear.
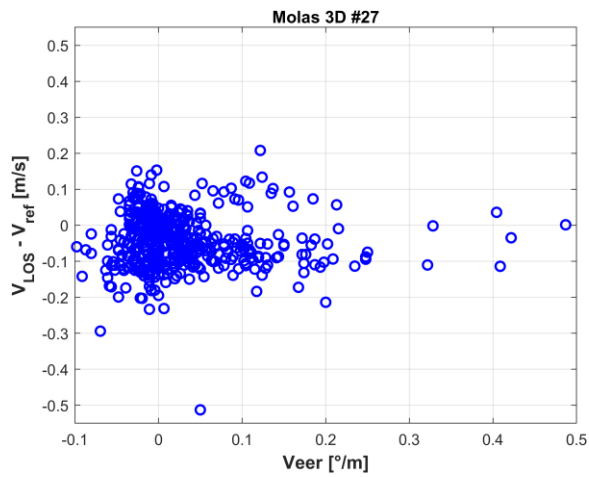
Figure 6.1.15 Deviations against veer.
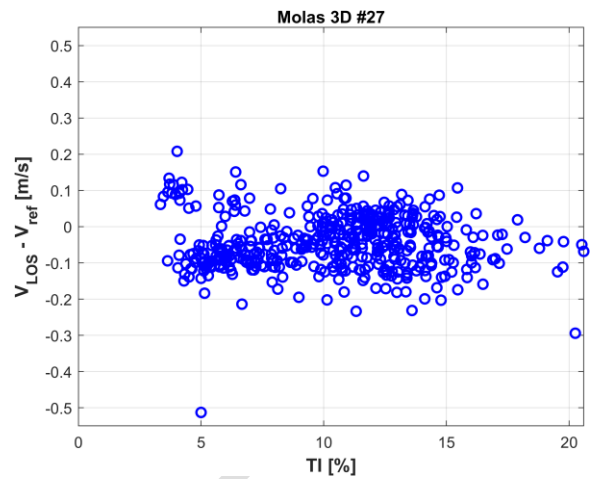
Figure 6.1.16 Deviations against TI.
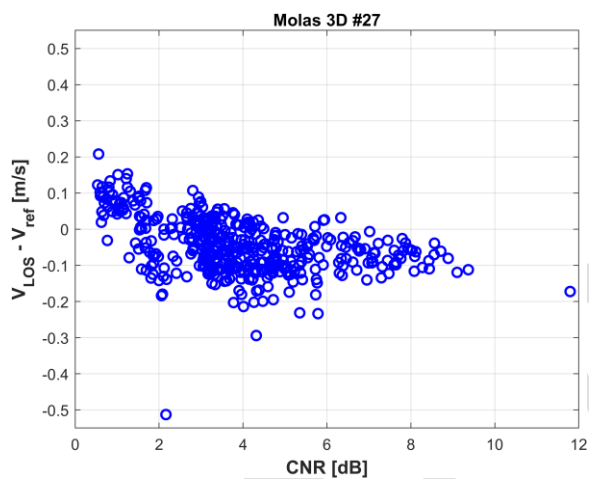
Figure 6.1.17 Deviations against CNR.
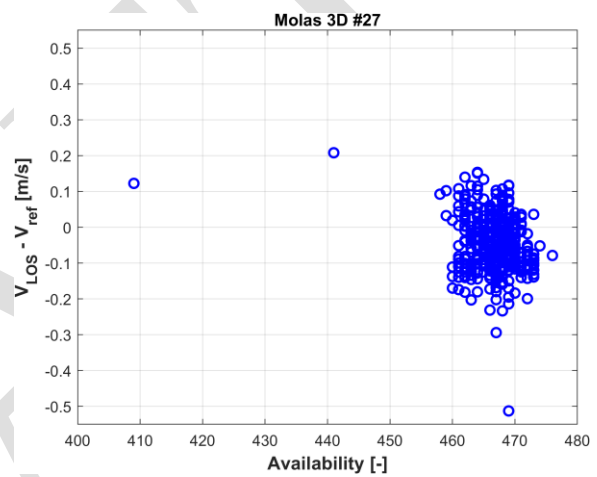
Figure 6.1.18 Deviations against lidar availability.

6.1.3 Binned dataset

Figure 6.1.19 shows the binned linear regression. The bins are formed based on the reference wind speed with a bin width of 0.5m/s and centered at multiples of 0.5m/s. Figure 6.1.20 shows the deviations relative to the reference uncertainty with coverage factor $k = 2$. The method applied to estimate this uncertainty component is outlined in Appendix B.
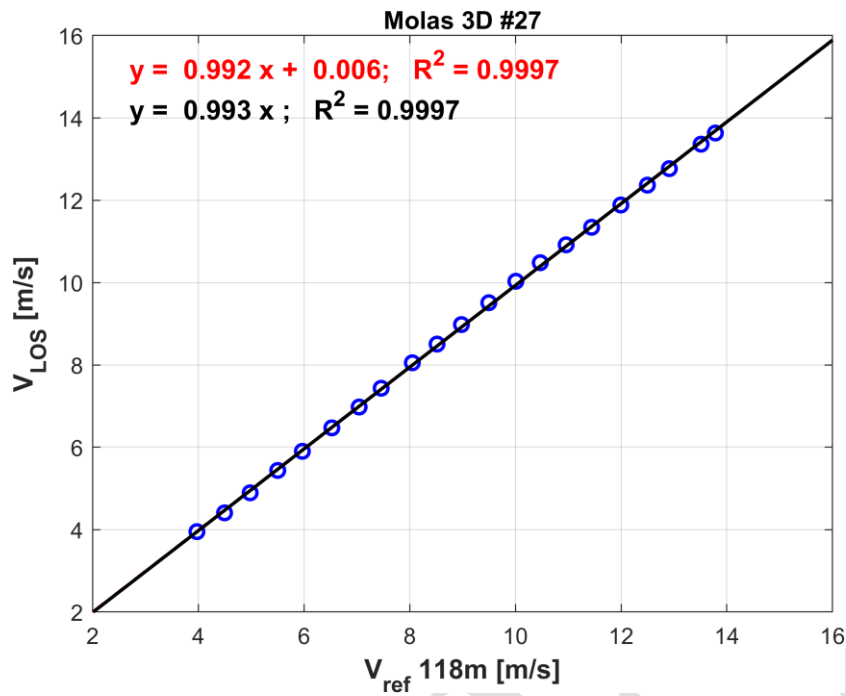
Figure 6.1.19 Linear regression of binned dataset.
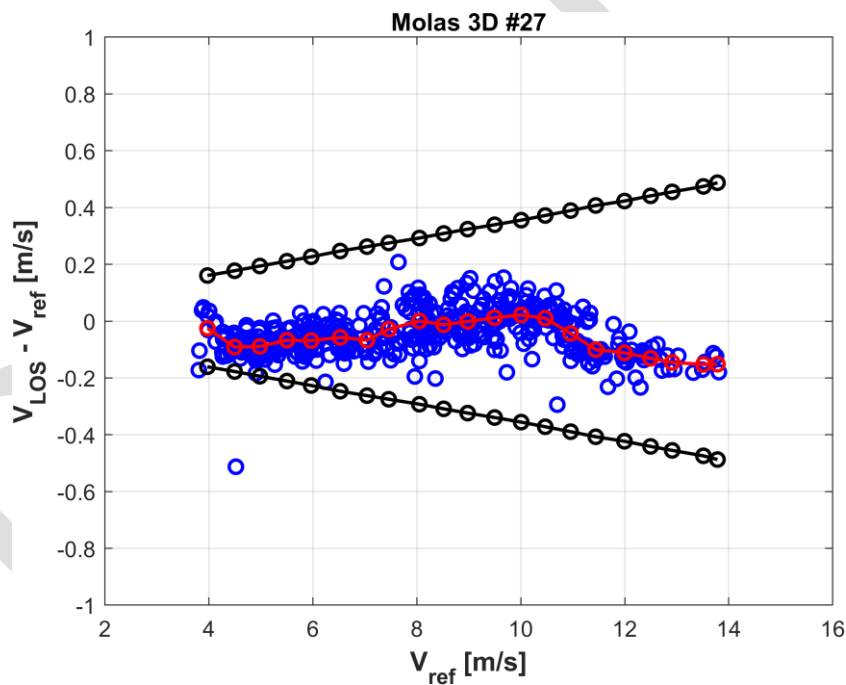
Figure 6.1.20 Deviations against reference wind speed. Each blue dot represents a 10min. value; the red dots are the deviations bin averages, and the black dots show $\pm 2u_{ref}$ which is the reference uncertainty with coverage factor $k = 2$.
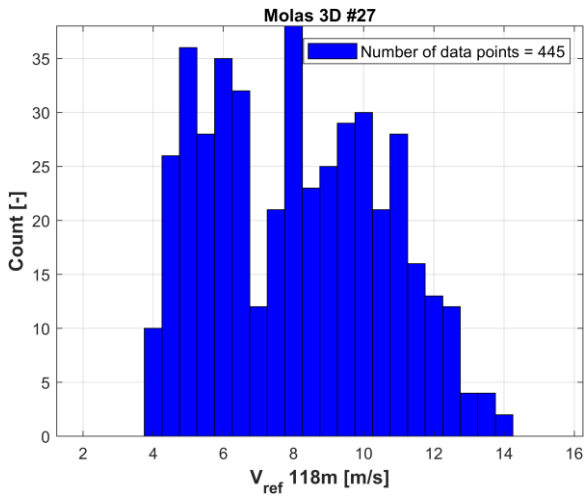
Figure 6.1.21 Distribution of the 10min.reference wind speed during the period.
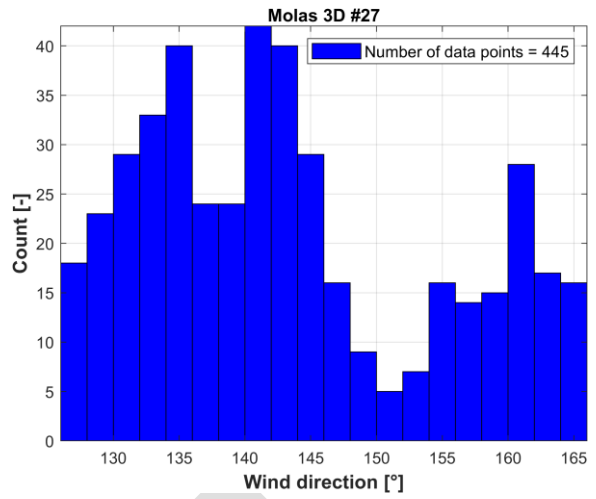
Figure 6.1.22 10min. wind direction distribution during the period.
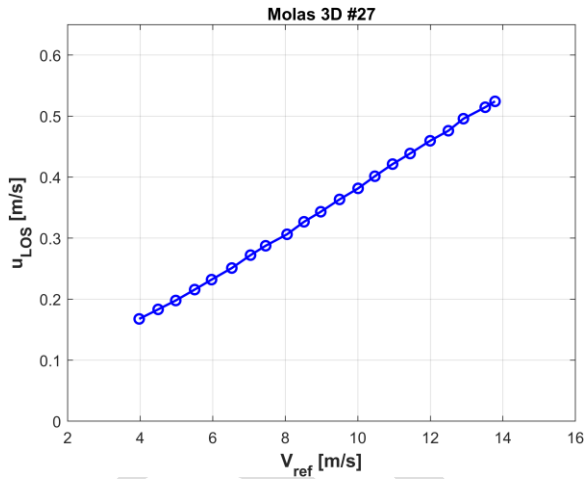
Figure 6.1.23 Standard uncertainty with ($k = 2$) in m/s against reference wind speed.
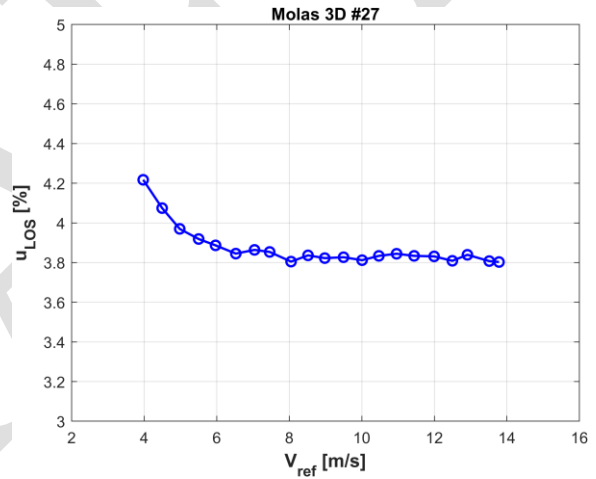
Figure 6.1.24 Standard uncertainty with ($k = 2$) in percentage against reference wind speed.

Table 6.1 Binned dataset and uncertainty results.

Bin	N	V_{hor}	V_{ref}	V_{los}	ΔV	σ_{dev}	θ_{r_i}	u_{Vhor}	f_{A1}	f_{A2}	f_{A3}	u_{Vref}	u_{LOS}, k=1	u_{LOS}, k=2	u_{LOS}, k=2
[-]	[-]	[m/s]	[m/s]	[m/s]	[m/s]	[m/s]	[deg]	[m/s]	[-]	[m/s]	[m/s]	[m/s]	[m/s]	[m/s]	[%]
7	10	4.13	3.97	3.95	-0.02	0.07	-9.99	0.08	0.98	-0.43	0.71	0.08	0.08	0.17	4.22
8	26	4.64	4.50	4.41	-0.09	0.09	-3.28	0.09	0.99	-0.49	0.26	0.09	0.09	0.18	4.07
9	36	5.16	4.98	4.89	-0.09	0.04	-2.28	0.10	0.99	-0.55	0.20	0.10	0.10	0.20	3.97
10	28	5.69	5.50	5.44	-0.07	0.03	-2.42	0.11	0.99	-0.61	0.24	0.11	0.11	0.22	3.92
11	35	6.18	5.97	5.90	-0.07	0.05	1.39	0.11	0.99	-0.66	-0.15	0.11	0.12	0.23	3.89
12	32	6.80	6.53	6.47	-0.06	0.04	1.21	0.12	0.99	-0.73	-0.14	0.12	0.13	0.25	3.85
13	12	7.29	7.04	6.98	-0.07	0.06	4.16	0.13	0.99	-0.77	-0.53	0.13	0.14	0.27	3.86
14	21	7.68	7.46	7.43	-0.03	0.08	4.01	0.14	0.99	-0.82	-0.53	0.14	0.14	0.29	3.85
15	38	8.21	8.05	8.05	0.00	0.07	-1.44	0.15	0.99	-0.87	0.20	0.15	0.15	0.31	3.80
16	23	8.70	8.52	8.51	-0.01	0.07	1.64	0.16	0.99	-0.93	-0.25	0.15	0.16	0.33	3.84
17	25	9.16	8.98	8.98	0.00	0.07	0.04	0.16	0.99	-0.98	-0.01	0.16	0.17	0.34	3.82
18	29	9.63	9.50	9.51	0.01	0.07	-3.30	0.17	0.99	-1.03	0.55	0.17	0.18	0.36	3.83
19	30	10.13	10.01	10.03	0.02	0.06	-3.76	0.18	0.99	-1.08	0.66	0.18	0.19	0.38	3.81
20	21	10.65	10.47	10.48	0.01	0.08	-7.48	0.19	0.99	-1.13	1.38	0.19	0.20	0.40	3.83
21	28	11.19	10.96	10.92	-0.04	0.06	-8.29	0.20	0.98	-1.18	1.60	0.19	0.21	0.42	3.84
22	16	11.76	11.44	11.34	-0.10	0.06	-10.92	0.21	0.98	-1.23	2.22	0.20	0.22	0.44	3.83
23	13	12.19	11.99	11.88	-0.11	0.06	-7.17	0.21	0.99	-1.29	1.51	0.21	0.23	0.46	3.83
24	12	12.77	12.50	12.37	-0.13	0.04	-9.35	0.22	0.98	-1.34	2.06	0.22	0.24	0.48	3.81
25	4*	13.20	12.91	12.77	-0.15	0.03	-9.66	0.23	0.98	-1.39	2.20	0.23	0.25	0.50	3.84
26	4*	13.75	13.51	13.36	-0.15	0.03	-8.01	0.24	0.98	-1.45	1.91	0.24	0.26	0.51	3.81
27	2*	14.23	13.78	13.63	-0.15	0.04	-12.91	0.25	0.97	-1.48	3.16	0.24	0.26	0.52	3.80

*Incomplete bin (less than 5 points)

6.2 Molas 3D Unit 28

6.2.1 Filtering effects

Figure 6.2.1 and Figure 6.2.2 show the effect of the CNR filter on the time series data of the Molas 3D unit 27. The blue points pass the filter, and the red ones are excluded by the filter.
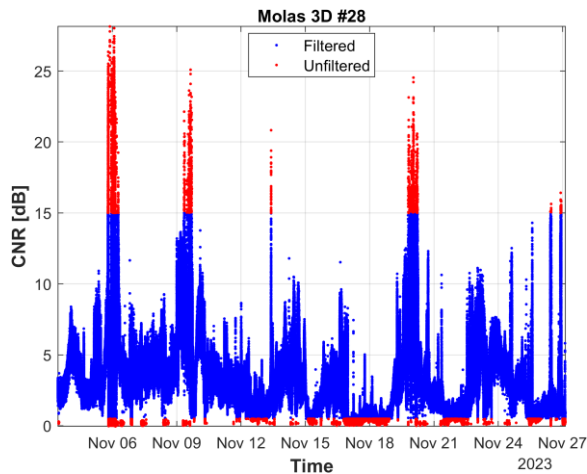
Figure 6.2.1 CNR filter.
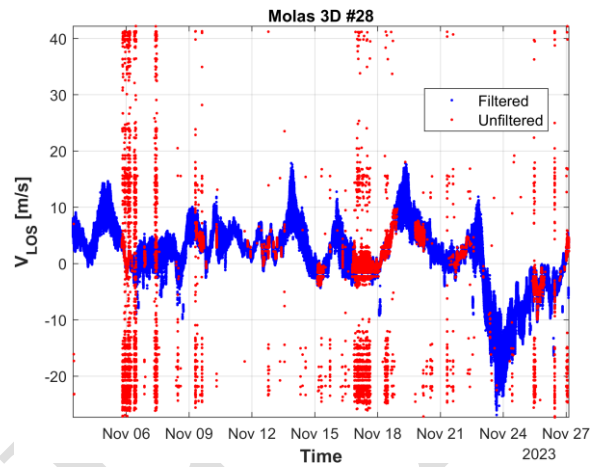
Figure 6.2.2 CNR filter effect on lidar LOS speed.

Figure 6.2.3 shows the independent effect of the wind speed filter on the data across the measurement period. The same is shown for temperature and wind direction in Figure 6.2.4 and Figure 6.2.5 respectively. Additionally, Figure 6.2.6 shows the lidar-cup deviation with varying wind direction to confirm the selected sector is valid.
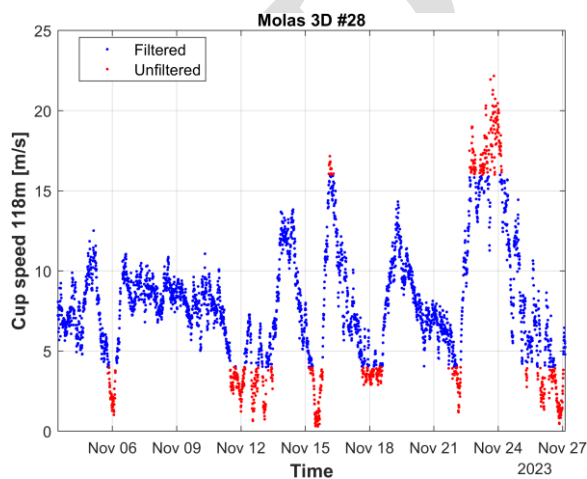
Figure 6.2.3 Cup wind speed filter.
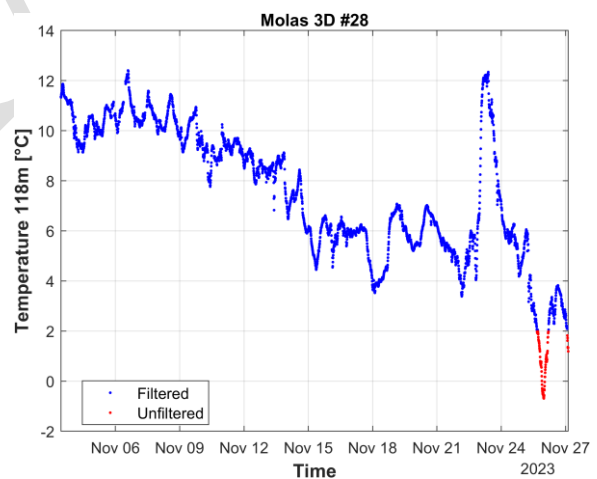
Figure 6.2.4 Temperature filter.
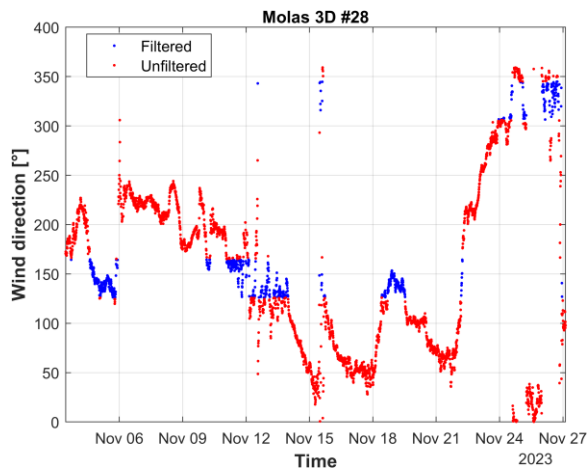
Figure 6.2.5 Wind direction filter.
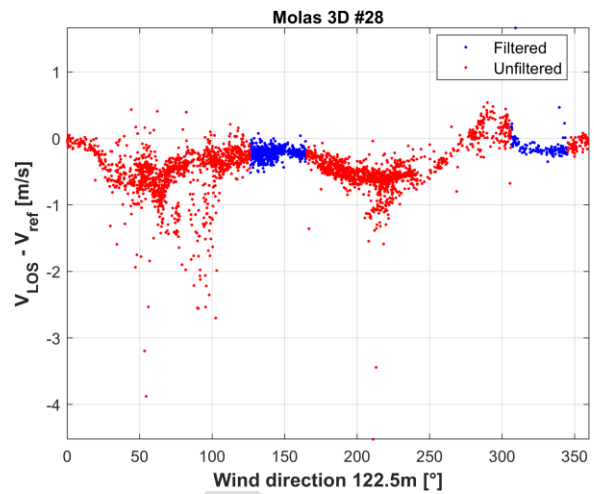
Figure 6.2.6 Wind direction filter and error.

Figure 6.2.7 shows the availability of the lidar over time. The filter was set to exclude 10-minute periods where less than 400 data samples were obtained by the lidar. Contrary to unit 27, unit 28 did not show the same decrease in sampling rate at the end of the campaign. The calibration datasets are therefore different for both lidars as they include different data periods. This also leads to different wind conditions in the results of lidar units 27 and 28. For example, the dataset of unit 28 includes wind direction from north-west as this period was not removed by the availability filter.
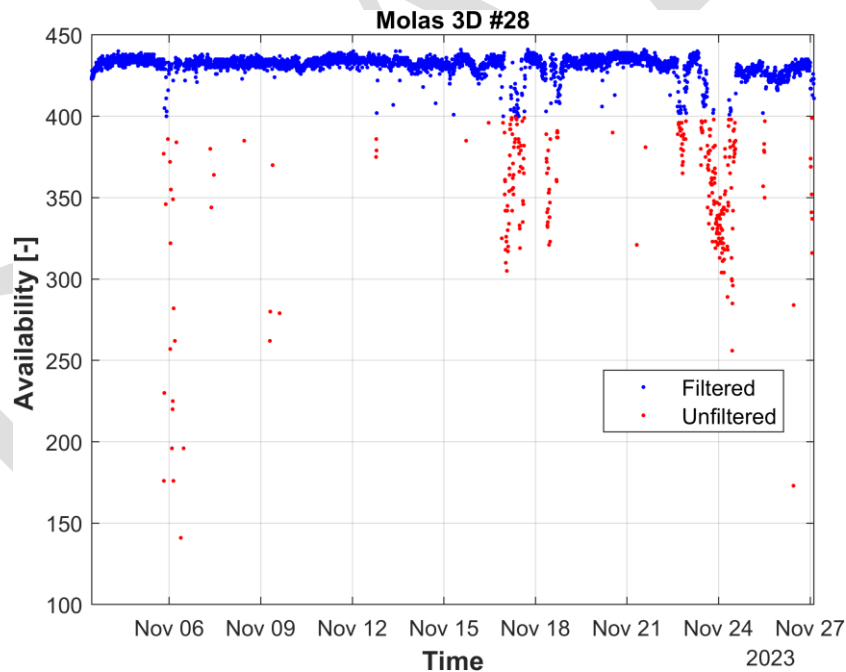
Figure 6.2.7 Lidar availability filter.

6.2.2 10-minute average dataset

Figure 6.2.8 shows the linear regression obtained between the lidar line-of-sight wind speed and the reference wind speed. Note that the reference wind speed may both be negative and positive due to the projection onto the line-of-sight, positive for wind directions aligned with the LOS direction (θ_{los}) and negative for wind directions in the opposite direction ($\theta_{los} + 180$). The linear fit with and without forced y-intercept are also displayed, together with their respective coefficient of determination.

Figure 6.2.9 to Figure 6.2.18 show how the deviation (lidar-cup) evolves with various measured parameters.
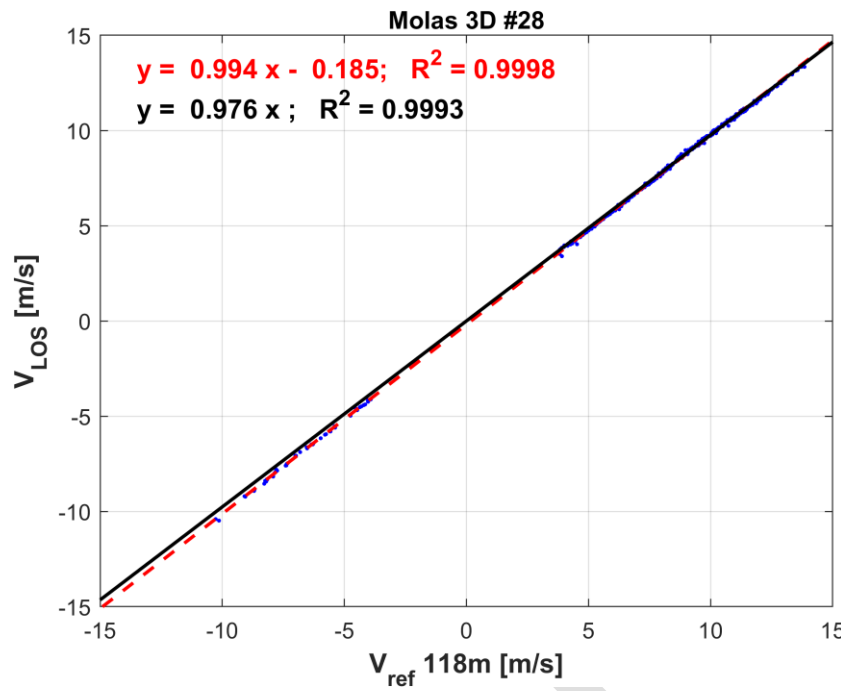
Figure 6.2.8 Linear regression of 10min. averages.
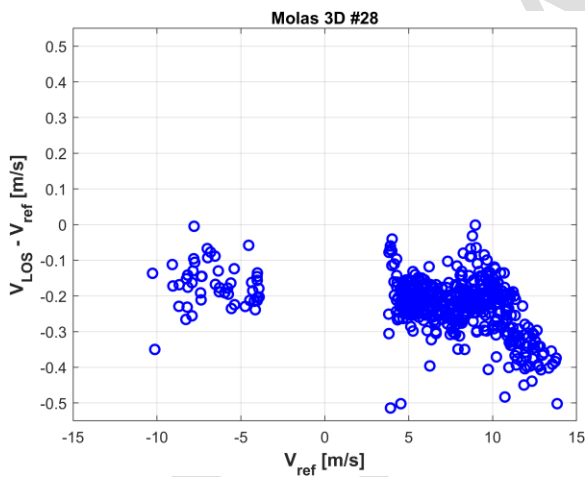
Figure 6.2.9 Deviations against reference wind speed.
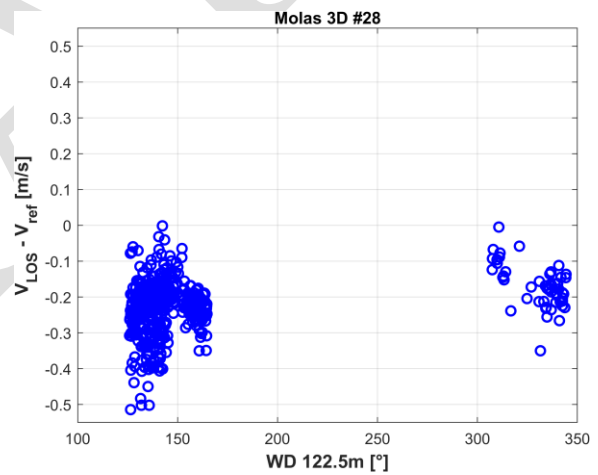
Figure 6.2.10 Deviations against wind direction.
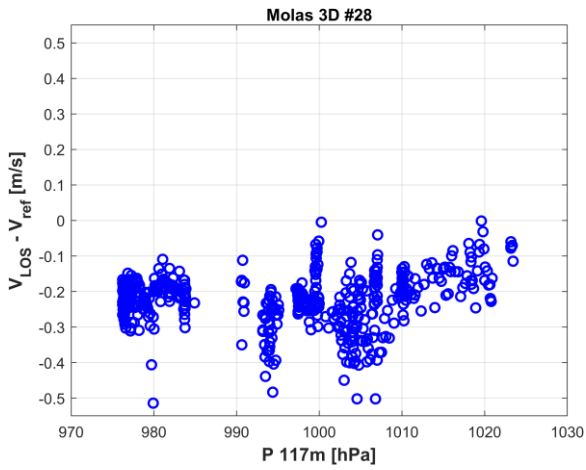
Figure 6.2.11 Deviations against air pressure.
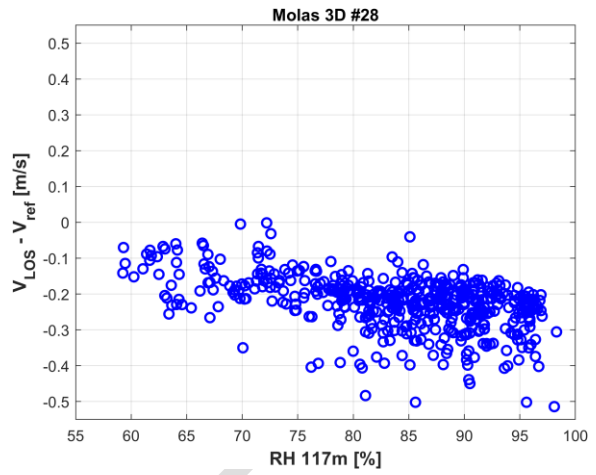
Figure 6.2.12 Deviations against relative humidity.
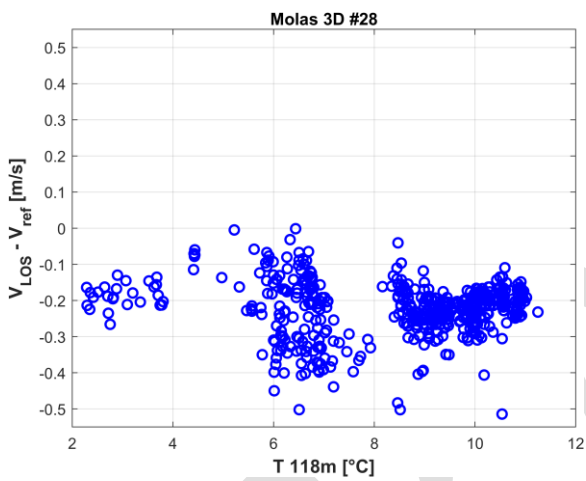
Figure 6.2.13 Deviations against temperature.
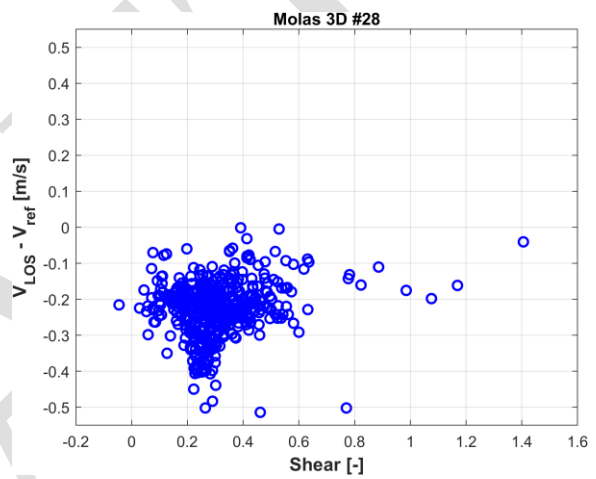
Figure 6.2.14 Deviations against shear.
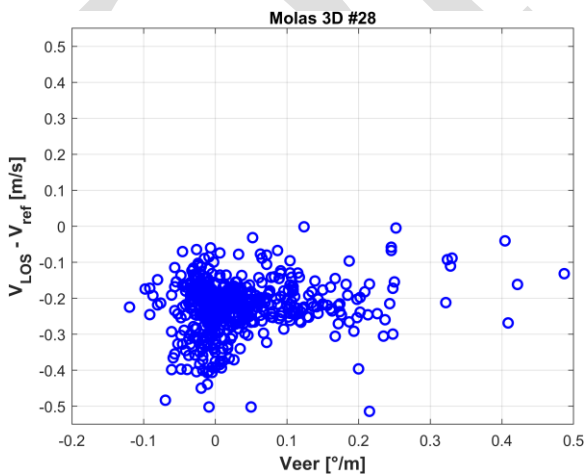
Figure 6.2.15 Deviations against veer.
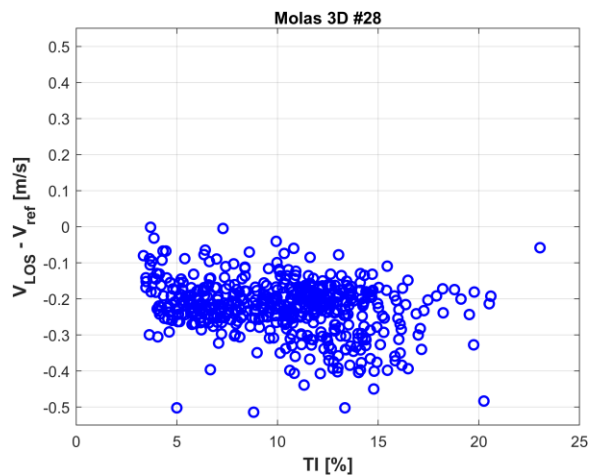
Figure 6.2.16 Deviations against TI.
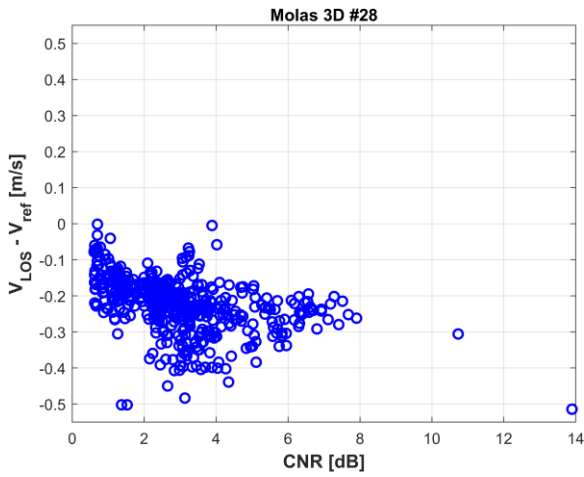
Figure 6.2.17 Deviations against CNR.   **Figure 6.2.18 Deviations against lidar availability.**
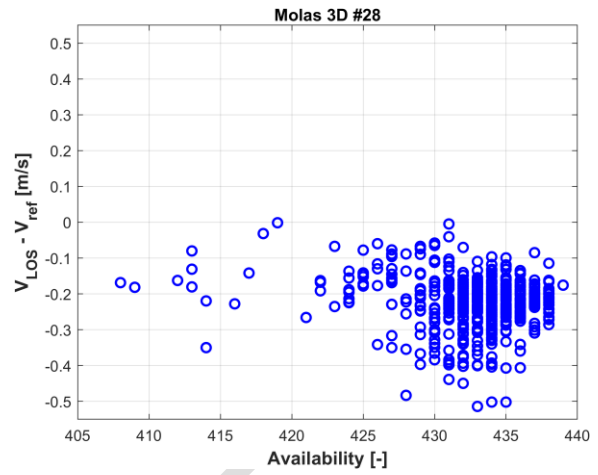
6.2.3 Binned dataset

Figure 6.2.19 shows the binned linear regression. The bins are formed based on the reference wind speed with a bin width of 0.5m/s and centered at multiples of 0.5m/s. Figure 6.2.20 shows the deviations relative to the reference uncertainty with coverage factor $k = 2$. The method applied to estimate this uncertainty component is outlined in Appendix B. Note that for the deviations and uncertainty calculation negative reference wind speed bins have been combined with positive ones. As seen from Figure 6.2.19 and Figure 6.2.20, the lidar measurements shows a small negative offset (-0.2m/s) relative to the cup, which may be corrected as a frequency offset or by correcting measured LOS speeds.
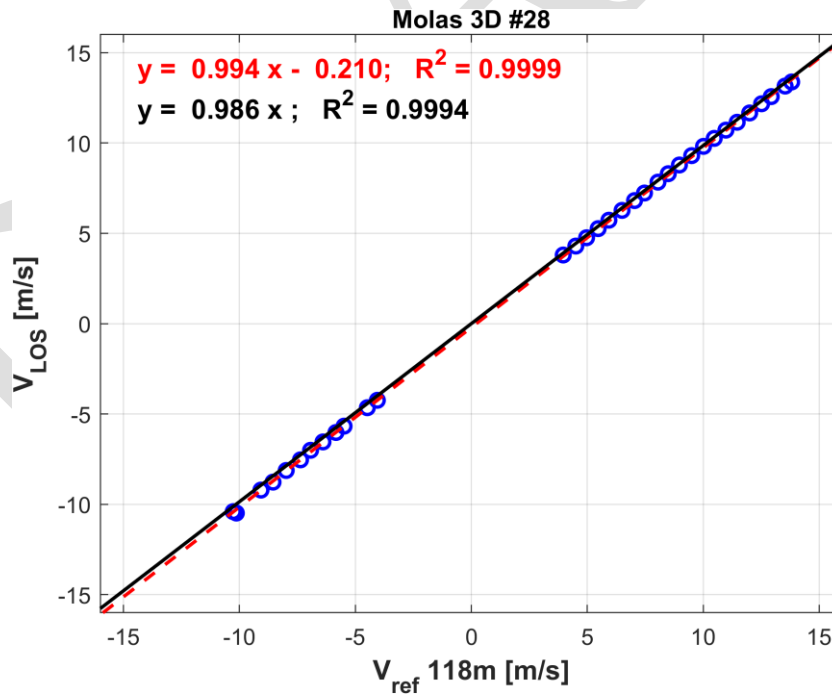
Figure 6.2.19 Linear regression of binned dataset.
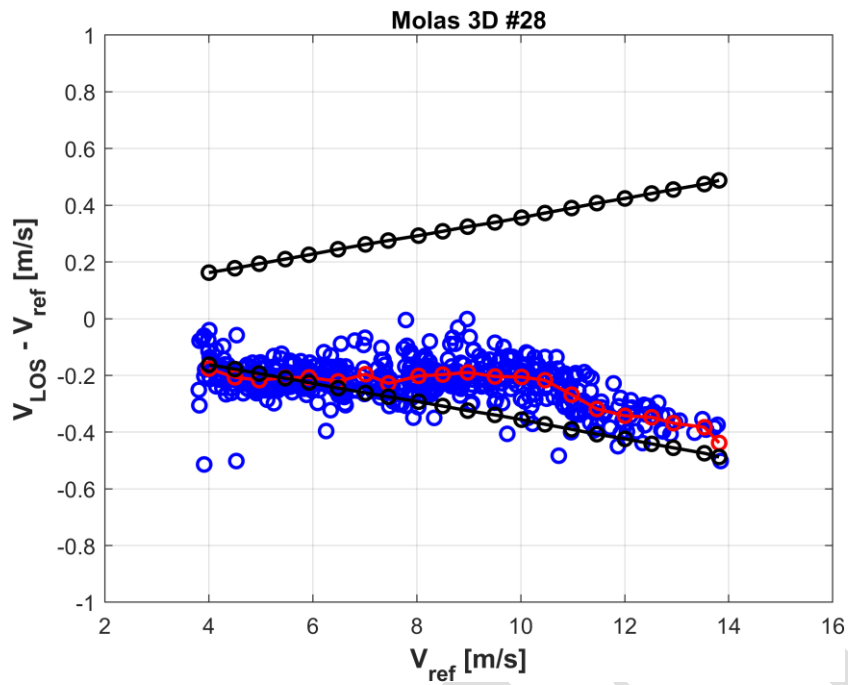
Figure 6.2.20 Deviations against reference wind speed. Each blue dot represents a 10min. value; the red dots are the deviations bin averages, and the black dots show $\pm 2u_{ref}$ which is the reference uncertainty with coverage factor $k = 2$.
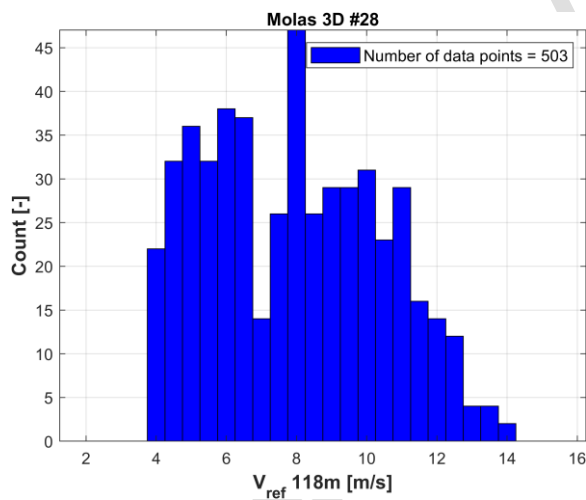
Figure 6.2.21 Distribution of the 10min.reference wind speed during the period.
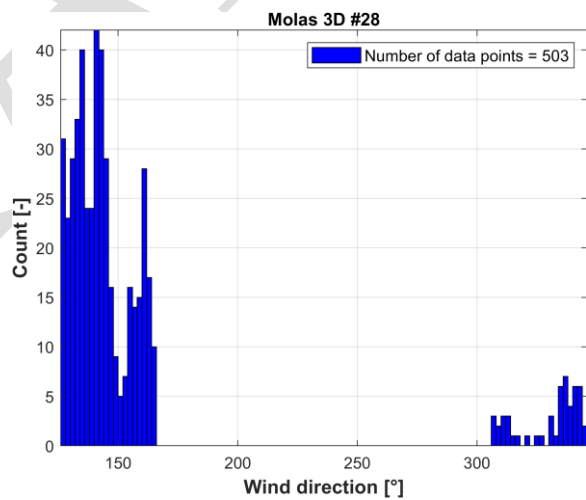
Figure 6.2.22 10min. wind direction distribution during the period.
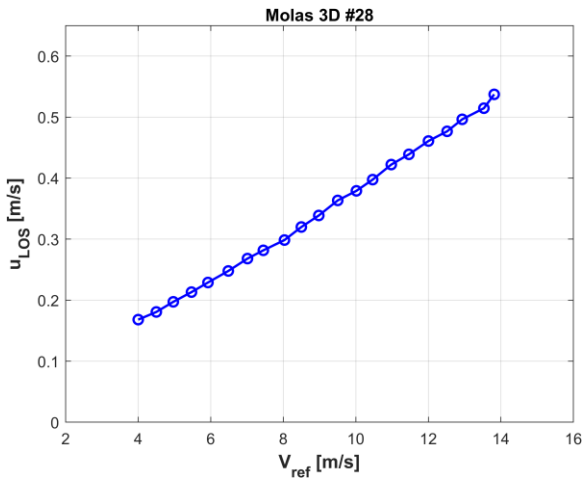
Figure 6.2.23 Standard uncertainty with ($k = 2$) in m/s against reference wind speed.
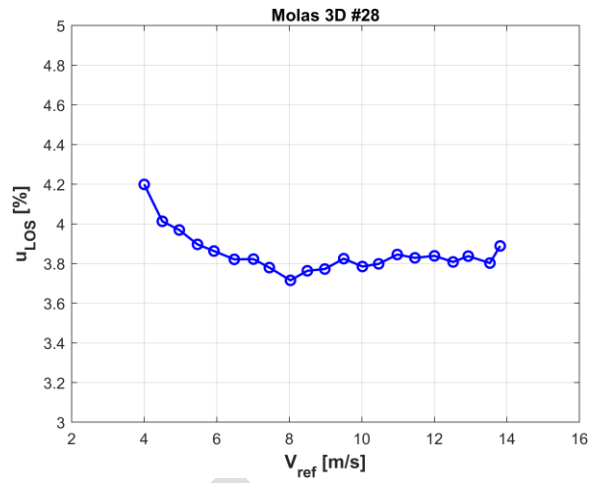
Figure 6.2.24 Standard uncertainty with ($k = 2$) in percentage against reference wind speed.

Table 6.2 Binned dataset and uncertainty results.

Bin	N	V_{hor}	V_{ref}	V_{los}	ΔV	σ_{dev}	θ_{r_i}	u_{Vhor}	f_{A1}	f_{A2}	f_{A3}	u_{Vref}	u_{LOS}, k=1	u_{LOS}, k=2	u_{LOS}, k=2
[-]	[-]	[m/s]	[m/s]	[m/s]	[m/s]	[m/s]	[deg]	[m/s]	[-]	[m/s]	[m/s]	[m/s]	[m/s]	[m/s]	[%]
7	22	4.145	4.004	4.000	-0.176	0.103	-2.012	0.082	0.994	-0.442	0.145	0.081	0.084	0.168	4.199
8	32	4.643	4.503	4.349	-0.207	0.071	-1.301	0.089	0.994	-0.496	0.105	0.089	0.090	0.181	4.013
9	36	5.152	4.971	4.754	-0.217	0.033	-1.861	0.097	0.994	-0.550	0.166	0.097	0.099	0.197	3.969
10	32	5.662	5.472	5.310	-0.208	0.040	-2.198	0.106	0.994	-0.604	0.216	0.105	0.107	0.213	3.897
11	38	6.134	5.926	5.749	-0.207	0.036	1.873	0.113	0.994	-0.655	-0.199	0.113	0.114	0.229	3.863
12	37	6.740	6.486	6.306	-0.221	0.056	-0.340	0.123	0.994	-0.720	0.040	0.122	0.124	0.248	3.821
13	14	7.265	7.015	6.853	-0.196	0.069	-0.938	0.132	0.994	-0.776	0.118	0.131	0.134	0.268	3.822
14	26	7.697	7.452	7.277	-0.228	0.052	5.706	0.139	0.989	-0.818	-0.761	0.138	0.141	0.282	3.780
15	47	8.216	8.034	7.894	-0.202	0.065	-2.184	0.147	0.994	-0.877	0.311	0.146	0.149	0.299	3.715
16	26	8.687	8.500	8.353	-0.197	0.063	3.464	0.155	0.992	-0.926	-0.522	0.154	0.160	0.320	3.764
17	29	9.175	8.980	8.811	-0.189	0.072	0.154	0.163	0.994	-0.980	-0.024	0.162	0.169	0.339	3.772
18	29	9.634	9.503	9.299	-0.204	0.066	-2.705	0.171	0.993	-1.028	0.452	0.170	0.182	0.363	3.825
19	31	10.147	10.017	9.834	-0.206	0.063	-3.141	0.179	0.993	-1.082	0.553	0.178	0.190	0.379	3.785
20	23	10.656	10.466	10.261	-0.217	0.073	-5.919	0.188	0.989	-1.132	1.093	0.186	0.199	0.398	3.798
21	29	11.206	10.978	10.710	-0.268	0.057	-8.084	0.197	0.984	-1.185	1.567	0.195	0.211	0.422	3.846
22	16	11.763	11.465	11.146	-0.318	0.057	-10.329	0.206	0.978	-1.236	2.097	0.204	0.219	0.439	3.829
23	14	12.228	12.003	11.661	-0.342	0.059	-7.460	0.214	0.986	-1.295	1.578	0.212	0.230	0.461	3.839
24	12	12.770	12.517	12.170	-0.348	0.045	-8.759	0.223	0.983	-1.348	1.933	0.221	0.238	0.477	3.808
25	4*	13.195	12.934	12.565	-0.368	0.028	-9.067	0.230	0.982	-1.391	2.068	0.228	0.248	0.496	3.837
26	4*	13.753	13.532	13.149	-0.383	0.020	-7.417	0.239	0.986	-1.456	1.765	0.237	0.257	0.515	3.802
27	2*	14.225	13.815	13.377	-0.438	0.090	-12.317	0.247	0.971	-1.484	3.017	0.244	0.269	0.537	3.889

*Incomplete bin (less than 5 points)

7. References

1. IEC 61400-50-3, February 2022.
2. MEASNET Anemometer calibration procedure. Version 3. December 2020.
3. CUP ANEMOMETER CLASSIFICATION WindSensor P2546-OPR. DTU Wind Energy, Rev. 04, 2020-03-06.

Appendix A Calibration certificates

A.1 Cup anemometer 118m

Svend Ole Hansen ApS

SCT. JØRGENS ALLÉ 5C · DK-1615 KØBENHAVN V · DENMARK
TEL: (+45) 33 25 38 38 · WWW.SOHANSEN.DK

WIND
ENGINEERING
FLUID
DYNAMICS

CERTIFICATE OF CALIBRATION

1103/4667

Calibrated item

Type	WindSensor P2546D-OPR Cup Anemometer
Serial no.	67079
Manufacturer	WindSensor, Frederiksborgvej 399, 4000 Roskilde Denmark
Item received	April 01, 2022
Remarks	-

Calibration

Calibration institute	Svend Ole Hansen ApS, Sct. Jørgens Allé 5C, DK-1615 København V
Procedure	IEC 61400-12-1:2017, Annex F
Client	WindSensor, Frederiksborgvej 399, 4000 Roskilde Denmark
Calibrated by	Calibrator, olm
Date of calibration	April 02, 2022
Approved by	Calibration engineer, sfo
Post calibration	No
Re-calibration due	-

Certificate

Certificate no.	22.02.05383
Date of issue	April 05, 2022
Issued by	ca
Number of pages	4

Accreditation

Accredited to ISO 17025:2017 by DANAK. DANAK is signatory to the European co-operation for Accreditation (EA) Multilateral Agreement and to the International Laboratory Accreditation Cooperation (ILAC) Mutual Recognition Arrangement.

The calibration institute is approved by MEASNET and IECRE.

DANAK CAL Reg.nr. 452

VAT no. DK 11 16 20 37

PAGE 1 OF 4

Calibration conditions

Turbulence intensity	1-2 % (alongwind)
Air temperature	27.4 °C (average value)
Barometric pressure	1017.8 hPa (average value)
Relative humidity	19.7 % (average value)
Air density	1.18 kg/m^3 (average value)
Flow inclination	< 0.2°
Anemometer yaw orientation	Not relevant
Remarks	(none)

Calibration results

Calibration equation v [m/s] = 0.61957· f [Hz] + 0.21074

The calibration equation is obtained from a linear regression of the reference air velocity upon the Device Under Test (DUT) output. The residual is the deviation of the calibration equation prediction from the reference air velocity.

The calibration results relate only to the calibrated item.

Succession #	Velocity pressure [Pa]	Air temperature [°C]	Air density [kg/m^3]	Ref. air velocity, v [m/s]	Uncertainty u_c ($k=2$) [m/s]	DUT output Frequency, f [Hz]	Residual, d [m/s]
2	10.11	27.4	1.18	4.145	0.025	6.3547	-0.003
4	15.38	27.5	1.18	5.114	0.028	7.9184	-0.003
6	22.18	27.4	1.18	6.140	0.033	9.5582	0.008
8	29.68	27.3	1.18	7.102	0.037	11.1183	0.003
10	38.41	27.3	1.18	8.079	0.041	12.7092	-0.006
12	48.34	27.2	1.18	9.062	0.046	14.3029	-0.010
13-last	59.34	27.2	1.18	10.040	0.050	15.8650	0.000
11	71.47	27.3	1.18	11.020	0.055	17.4113	0.021
9	84.79	27.3	1.18	12.004	0.059	19.0310	0.002
7	99.34	27.4	1.18	12.995	0.064	20.6513	-0.011
5	115.27	27.5	1.18	14.000	0.069	22.2563	0.000
3	132.19	27.5	1.18	14.993	0.073	23.8644	-0.004
1-first	147.78	27.3	1.18	15.846	0.077	25.2313	0.003

Visual presentation of calibration results
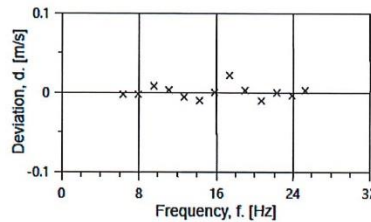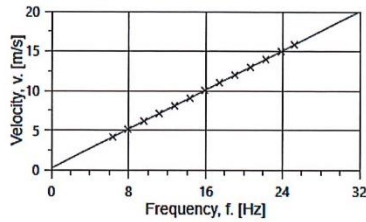
Linear regression results

Method	Least squares linear regression
Slope	0.61957 (m/s)/Hz
Offset	0.21074 m/s
Coefficient of correlation	$\rho = 0.999998$
Standard error of estimate	0.0087 m/s
Slope standard error	0.00041 (m/s)/Hz
Offset standard error	0.00687 m/s
Slope and offset covariance	-0.000002611 (m/s)^2/Hz
Remarks	Linearity complies with IEC 61400-12-1:2017, Annex F.

Uncertainties

The uncertainties stated under *Calibration results* relate to the reference air velocity at each calibration point. The uncertainty is the total combined uncertainty at 95 % confidence level (coverage factor $k = 2$) in accordance with EA-4/02. The uncertainty complies with the requirements in IEC 61400-12-1:2017, Annex F. The uncertainty due to the wind tunnel correction function has been documented to be 0.1 % ($k = 2$).

The slope and offset uncertainties and their covariance stated under *Linear regression results* are related to the linear regression only, and do not relate to the reference air velocity uncertainties. The slope and offset uncertainties have $v = 11$ degrees of freedom.

Calibration wind tunnel

ID	DK1
Test section	Octagonal, hxw = 1.20x1.75 m
Effective area of test section	2.10 m^2
Setup report	SOH document no. 18.1.001
Blockage ratio*	~1.0 % (Anemometer and mounting pole)

* The effect of blockage is taken into account in the calibration results.

Equipment used

Function	ID	Model / comments	Re-calibration due
QC Anemometer	11641	11641	-
Mounting	-	Mounting tube, diameter = 25 mm	-
Tunnel Temperature	T4	PT100 Temperature sensor	2023-04-06
Differential Pressure	1501197	FCO560 Pressure manometer	2023-03-24
Relative Humidity	Z0420014	HMW71U Humidity transmitter	2023-04-06
Barometric Pressure	U4220037	PTB100A Analogue barometer	2023-04-12
Pitot tube	A37AB	Ellipsoidal tip pitot tube	2027-02-22
Data acquisition	1A841F0	Computer Board: ME-REDLAB 1608GX.	-
Computer	-	PC dedicated to data acquisition	-

Calibrations of the relevant equipment are carried out by external accredited institutions, and are traceable to national standards. A real-time analysis module within the data acquisition software detects pulse frequency.

Setup photo

The shown anemometer is of the same type as the one calibrated.
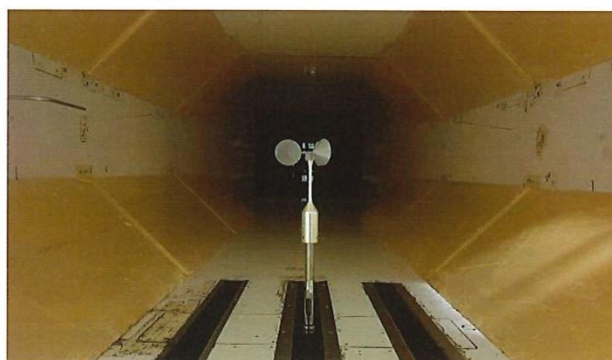
End of certificate

Appendix B Uncertainty analysis

This section represents the uncertainty budget for the line-of-sight measured wind speeds. The analysis is based on binned data (binning is based on the reference wind speed). All uncertainties are calculated for a coverage factor k=1 and multiplied by 2 to give a coverage factor k=2 (95% confidence limit).

B.1 Reference wind speed uncertainties

Here we followed the requirements in [1]. The combined uncertainty on the reference wind speed $Vref$ is:

$$u_{Vref} = \sqrt{\left(\frac{\partial V_{ref}}{\partial V_{hor}} u_{Vhor}\right)^2 + \left(\frac{\partial V_{ref}}{\partial \varphi} u_{\varphi}\right)^2 + \left(\frac{\partial V_{ref}}{\partial \theta_r} u_{\theta_r}\right)^2}$$

The sensitivity coefficients for u_{Vhor}, u_{φ} and u_{θ_r}, denoted f_{A1}, f_{A2} and f_{A3} respectively, are calculated for each bin:

$$f_{A1} = \cos \varphi * \cos (\theta_{r_i})$$
$$f_{A2} = -\sin \varphi * V_i * \cos (\theta_{r_i})$$
$$f_{A3} = -\sin(\theta_{r_i}) * \cos \varphi * V_i$$

...where θ_{r_i} is the bin average of the absolute value of the relative wind direction.

The combined uncertainty u_{Vref} is thus:

$$u_{Vref} = \sqrt{(f_{A1} * u_{Vhor})^2 + (f_{A2} * u_{\varphi})^2 + (f_{A3} * u_{\theta_r})^2}$$

B.1.1 Horizontal wind speed uncertainty

The uncertainty of V_{hor}, u_{Vhor}, is the combination of the reference wind speed sensor (cup anemometer) uncertainty (u_{sens}) and the uncertainty due to the fact that the reference is not measuring exactly in the same volume as the LOS being calibrated (u_{pos}):

$$u_{Vhor} = \sqrt{u_{sens}^2 + u_{pos}^2}$$

The uncertainties of the reference cup anemometer were calculated according to IEC 61400-50-3:2022:

$$u_{sens} = \sqrt{u_{cal}^2 + u_{ope}^2 + u_{mast}^2 + u_{daq}^2 + u_{lgt}^2}$$

- Cup calibration uncertainty: we considered the cup calibration uncertainties due to wind tunnel calibration and traceability as two separate components:
    - u_{cal1} is the wind tunnel calibration standard uncertainty (k=1). This can be found in the Appendix A with a coverage factor of 2. For uncertainties where wind speed bins did not match the wind speeds from the certificates, interpolation was performed.

    - u_{cal2} is the standard error representing the spread of results from Measnet accredited wind tunnel. Measnet states that calibration results (i.e. the true wind speed corresponding to a given cup rotational speed) from the tunnels are within ±1% [2].

Consequently, assuming a uniform distribution of wind tunnel errors with a half width of 1%, $u_{cal2} = \frac{0.01}{\sqrt{3}} * V_i$

u_{cal1} and u_{cal2} are added in quadrature: $u_{cal}^2 = u_{cal1}^2 + u_{cal2}^2$

- The operational uncertainty of the cup anemometer u_{ope} was calculated according to:

$$u_{ope} = \frac{c}{\sqrt{3}}(0.05 \ m/s + 0.005 \cdot V_i)$$

...where the class number c for the WindSensor P2546D-OPR cup anemometer used is $c = 1.04$. This value corresponds to class A for this specific cup model [3]. The conditions on site have been verified for the duration of the campaign and correspond to the conditions for which this class is valid.

- Cup anemometer mounting uncertainty, $u_{mast} = 1.5\% * V_i$.
- Data acquisition system uncertainty, $u_{daq} = 0.2\% * V_i$ [1].
- There is no lightning filial at the mast top, thus $u_{lgt} = 0$.

The uncertainties due to the relative position and different measurement volume of the reference sensor compared to the probe volume of the calibrated LOS are expressed as:

$$u_{pos} = \sqrt{u_{probe}^2 + u_{inc}^2 + u_{vert\_pos}^2}$$

- Uncertainty due to the horizontal wind flow variation within the lidar probe volume due to terrain, based on available measurements at the site is $u_{probe} = 0.006\% * V_i$
- Inclined beam and range uncertainty, $u_{inc} = \alpha \frac{\sin\varphi u_{range}}{H_{ref}} V_{hor} = 0.11\% * V_i$; a range uncertainty $u_{range} = 4$m was used, as well as a shear value $\alpha = 0.3$, representative for this site / the average shear value during the calibration.
- Beam vertical position uncertainty, $u_{vert\_pos} = \alpha \frac{u_H}{H_{ref}} V_{hor} = 0.24\% * V_i$; a height uncertainty $u_H = 0.92$m. This is the expected height difference between the cup and lidar measurement point.

B.1.2 Relative wind direction uncertainty

The uncertainty of the relative wind direction is:

$$u_{\theta_r} = \sqrt{u_\theta{}^2 + u_{\theta_{los}}{}^2}$$

Where:
- The uncertainty of the wind direction sensor in the measurement sector is the combined uncertainties related to the calibration of the wind direction sensor and the influence of the met mast on the wind direction measurements, $u_\theta = 0.8°$
- The uncertainty of the determination of LOS direction was estimated as $u_{\theta_{los}} = 0.1°$

The components u_θ and $u_{\theta_{los}}$ were converted into radians.

B.1.3 Beam elevation angle uncertainty

The uncertainty of the beam elevation angle φ is assumed negligible as the elevation angle used is corrected based on GPS measurements. The accuracy of the GPS measurements was estimated to be +/- 3cm which is small compared to the reference height of 118m and measurement range of 1066m.

B.2 Flow inclination uncertainty

The uncertainty due to not including the vertical speed component (W) in the calculation of V_{ref} (in other words, disregarding the speed contribution due to the wind flow inclination angle, ψ) is:

$$u_\psi = W \sin\varphi = V_{hor} \tan\psi \sin\varphi$$

The inclination angle is obtained from the sonic measurement at 118m.

B.3 Uncertainty of the calibrated LOS speed

The uncertainty on the LOS wind speed was calculated as:

$$u_{LOS} = \sqrt{u_{ref}^2 + (V_{hor} \sin\varphi \cos\theta_r)^2 \left(u_\psi\right)^2 + \frac{\sigma_{dev}^2}{N}}$$

...where σ_{dev} is the standard deviation of the lidar deviations ($dev = V_{los} - V_{ref}f$) and N is the amount of data in each bin.